Bioresource Technology Reports 31 (2025) 102282

Contents lists available at ScienceDirect

Bioresource Technology Reports

journal homepage: www.sciencedirect.com/journal/bioresource-technology-reports

Prediction by a modified severity factor in $FeCl_3$-catalyzed hydrothermal fractionation of coconut husk: Enhancing hemicellulose hydrolysis and enzymatic digestibility of cellulose

Candra Wijaya [a], Ningsi Lick Sangadji [a], Maktum Muharja [a], Tri Widjaja [a], Lieke Riadi [b], Elaine Elaine [c], Raymond Lau [c], Arief Widjaja [a,*]

[a] Department of Chemical Engineering, Institut Teknologi Sepuluh Nopember, Kampus ITS Sukolilo, Surabaya, 60111, Indonesia
[b] Department of Chemical Engineering, Universitas Surabaya (UBAYA), Jalan Raya Kalirungkut (Tenggilis), Surabaya, 60293, Indonesia
[c] School of Chemistry, Chemical Engineering and Biotechnology, Nanyang Technological University, 62 Nanyang Drive, Singapore, 637459, Singapore

ARTICLE INFO

Keywords:
Coconut husk
Enzymatic hydrolysis
Ferric chloride
Hydrothermal pretreatment
Combined hydrolysis factor
Fractionation

ABSTRACT

Hydrothermal pretreatment (HTP) is essential for producing valuable hemicellulosic sugars and enhancing the enzymatic digestibility of lignocellulosic biomass for biofuel and biochemical production. However, conventional methods are often limited by high energy demands and low sugar yields. This study explores the catalytic role of ferric chloride ($FeCl_3$) as a less corrosive, high-catalytic activity, and cost-effective alternative to inorganic acids in the HTP of coconut husk (CCH), with the goal of improving hemicellulose hydrolysis and subsequent enzymatic conversion. The pretreatment was carried out at 120–180 °C with $FeCl_3$ concentrations ranging from 20 to 100 mM. A mathematically derived Combined Hydrolysis Factor (CHF) was applied to unify pretreatment conditions and correlate them with xylan hydrolysis, hemicellulosic sugar yield, compositional changes in CCH, and improvements in enzymatic digestibility. The results showed that $FeCl_3$-HTP enabled substantial to near-complete hemicellulose removal, exhibited a strong correlation between xylan removal and xylose release, and significantly enhanced enzymatic digestibility, as confirmed by XRD, SEM, and FTIR analyses. Mass balance analysis identified the optimal condition at 150 °C and 60 mM $FeCl_3$, yielding 22.04 g of total sugar per 100 g of raw CCH, 5.34 times higher than the yield from non-catalyzed pretreatment at the same temperature. These findings confirm the effectiveness of $FeCl_3$ as catalytic agent and establish CHF as a reliable predictive parameter for optimizing sugar recovery in scalable biomass conversion processes, highlighting its potential applicability to other lignocellulosic biomass as transferrable parameter under similar catalytic system, such as oil palm empty fruit bunches, for high-value bioproduct production.

1. Introduction

The depletion of fossil fuels and rising greenhouse gas emissions have intensified the urgency for renewable, environmentally responsible energy solutions (Rathour et al., 2023; Rodríguez-Rebelo et al., 2024). Lignocellulosic biomass is a widely available and versatile feedstock for sustainable biofuel and biochemical production (Basak et al., 2023; Gundupalli et al., 2022; Yaashikaa et al., 2022; Y. Zhang et al., 2023b). Among its components, hemicellulosic sugars, particularly xylose, can be converted to high-value xylitol, which offers health benefits and a market price (USD 5/kg) far above ethanol (USD 0.5/kg) (Felipe Hernández-Pérez et al., 2019). Incorporating xylitol into a biorefinery framework can therefore improve economic feasibility while diversifying products (Clauser et al., 2024).

In Indonesia, coconut husk (CCH), a byproduct of coconut processing, is abundant due to the globally leading production of 17.3 million tons of coconut fruit annually (Zikria, 2022). However, its high lignin content increases structural recalcitrance, limiting conventional fractionation efficiency (Vieira et al., 2024). Efficient recovery of cellulose, hemicellulose, and lignin from CCH is essential to maximize product yields and reduce waste. This requires advanced pretreatment methods capable of breaking lignin–carbohydrate linkages while preserving fermentable sugars, enabling CCH to serve as a competitive feedstock for integrated biofuel and biochemical production in lignocellulose-rich

* Corresponding author.
E-mail address: arief.widjaja@its.ac.id (A. Widjaja).

https://doi.org/10.1016/j.biteb.2025.102282
Received 1 July 2025; Received in revised form 26 August 2025; Accepted 29 August 2025
Available online 4 September 2025

tropical economies (Anuchi et al., 2022; Mankar et al., 2022; Muharja et al., 2018).

Pretreatment plays a critical role in breaking down the complex structure of recalcitrant biomass like CCH, making it accessible for enzyme attack or chemical conversion (Aline Otaviano et al., 2023). Traditional methods often use inorganic acids, such as sulfuric acid, which have significant drawbacks, including corrosive environments, not recoverable, and producing inhibitory by-products (Kininge and Gogate, 2022; R. Zhang et al., 2023a). Therefore, to overcome these drawbacks, metal salts, particularly ferric chloride ($FeCl_3$), have emerged as promising alternatives due to their lower corrosivity, higher selectivity, easy to recover, cheaper than inorganic acid, and ability to improve sugar yields without generating many inhibitors (Marecka-Migacz et al., 2020; Tang et al., 2022, 2021). Additionally, $FeCl_3$ exhibits higher catalytic activity than mineral acids at the same pH due to its Lewis acid properties, while presenting lower toxicity to biological systems, making it a promising catalyst for biomass pretreatment (Moodley et al., 2020).

Hydrothermal pretreatment (HTP), a commonly used method for producing hemicellulose fractions, is effective but often limited by high energy requirements, long reaction times, and relatively low sugar yields (Chen et al., 2022), underscoring the need for more efficient alternatives. $FeCl_3$, a low-cost metal salts, is hypothesized to enhance HTP by catalyzing selective hemicellulose hydrolysis, preserving cellulose, lowering reaction temperatures, and increasing enzymatic hydrolysis efficiency. While $FeCl_3$-HTP has been successfully applied to wheat straw, rapeseed straw, corn cob, and woody biomasses to enhance hemicellulose hydrolysis and enzymatic digestibility (Chen and Lee, 2020; Lu et al., 2025; Romero et al., 2018), the comprehensive pretreatment of CCH using $FeCl_3$ or other metal salts remains unexplored (Moodley et al., 2020). Moreover, optimizing this process requires a comprehensive understanding of key variables such as temperature, $FeCl_3$ concentration, and reaction time, which can be integrated into a combined hydrolysis factor (CHF) for streamlined analysis (Jiang et al., 2023; Y. Liu et al., 2024b). This modified severity factor more accurately describes xylan hydrolysis, conversion, and digestibility of biomass during HTP in the presence of catalytic agents such as inorganic acids, acid hydrotrope, and sulfites, compared to the conventional severity factor, which only accounts for pH and thus cannot capture catalytic effects beyond proton concentration (Jiang et al., 2023; Ma et al., 2018; Zhu et al., 2012). Although CHF analysis has been applied for certain reaction cases, the detailed kinetics underlying these interactions remain unclear, limiting the scalability of this approach for industrial applications (Lv et al., 2024; Ruiz et al., 2021).

Based on this background, this study investigates the fractionation of coconut husk (CCH) via $FeCl_3$-catalyzed hydrothermal pretreatment ($FeCl_3$-HTP). The modified Combined Hydrolysis Factor (CHF) is applied to evaluate the trade-offs between pretreatment severity and its effects on xylan degradation, biomass composition, and hemicellulosic sugar production. The impact of pretreatment on enzymatic hydrolysis is also assessed. The response of CHF is identified to guide effective process design and potential scale-up of CCH fractionation, with relevance to other lignocellulosic biomasses.

2. Materials and methods

2.1. Materials

The CCH biomass waste was collected from a traditional market in Surabaya, Indonesia. Meanwhile, oil palm empty fruit bunch (OPEFB) was collected from PT. Sawit Arum Madani, Blitar, Indonesia. Prior to use, it was rinsed and prepared according to NREL protocol (Hames et al., 2008), and ground mechanically to achieve a particle size of 40–60 mesh. The $FeCl_3{\cdot}6H_2O$ metal salt catalyst, of analytical-grade purity, was sourced from Merck, Germany. The cellulase enzyme, originating from *Trichoderma reesei* and other analytical-grade reagents were obtained from Sigma-Aldrich, USA.

2.2. $FeCl_3$-catalyzed HTP

The experimental procedure was adapted from prior research (Wijaya et al., 2025). To evaluate its efficiency in enhancing sugar production, $FeCl_3$-catalyzed HTP of CCH was conducted by varying the $FeCl_3$ concentration between 20 mM and 100 mM, and pretreatment temperature ranges between 120 °C to 180 °C. The fixed parameters such as the solid-to-liquid ratio and reaction duration were maintained at 1:20 and 30 min, respectively. Following HTP, the liquid hydrolysate was separated from the solid residues through vacuum filtration for further analysis. The efficiency of HTP in generating monomeric sugars such as glucose and hemicellulosic sugar were assessed using yield calculations, as outlined in Eqs. (1) and (2).

$$Y_{HS} = \frac{(xylose + galactose + arabinose + mannose)\ from\ hydrolysate\ \left(\frac{g}{L}\right)}{(xylose + galactose + arabinose + mannose)\ of\ CCH\ at\ 100\%conversion\ \left(\frac{g}{L}\right)} \quad (1)$$

$$Y_G = \frac{glucose\ from\ hydrolysate\ \left(\frac{g}{L}\right)}{glucose\ of\ CCH\ at\ 100\%conversion\ \left(\frac{g}{L}\right)} \quad (2)$$

where, Y_{HS} and Y_G are hemicellulosic sugar and glucose yield from liquid hydrolysate, respectively. The energy aspect of $FeCl_3$-catalyzed HTP of CCH was evaluated by recording the electrical energy consumption during the pretreatment process. Measurements were obtained using a kWh meter (PZEM-061, Peace Fair, China).

2.3. Mathematical reaction model

The kinetics of CCH hydrolysis during $FeCl_3$ pretreatment were modeled using a second-order rate expression, assuming first-order dependence on both the biomass (xylan component) and the $FeCl_3$ catalyst. The rate of xylan hydrolysis was described by the following Eq. (3) (Jiang et al., 2023; Ma et al., 2018; Zhu et al., 2012).

$$\frac{dX_{res}}{dt} = -k(T, C, \ldots)CX_{res} \quad (3)$$

where X_{res} is the residual xylan content in the pretreated solid, T is the temperature (K), C is the $FeCl_3$ concentration (mol/L), and $(k(T, C, \ldots))$ is the reaction rate constant, which depends on temperature, catalyst concentration which in this study, $FeCl_3$, and other factors.

The rate constant (k) was modeled using an Arrhenius-type equation, incorporating the influence of $FeCl_3$ concentration, as represented in Eq.

(4) (Jiang et al., 2023; Springer, 1966; Zhu et al., 2012).

$$k = \exp\left(\alpha - \frac{E_a}{RT} + \beta C\right) \tag{4}$$

where E_a is the apparent activation energy (kJ/mol), R is the universal gas constant (8.314 J/mol·K), and α and β are empirically determined constants.

For a given time t, the combined hydrolysis factor (CHF) was defined as Eq. (5).

$$CHF = \exp\left(\alpha - \frac{E_a}{RT} + \beta C\right) Ct \tag{5}$$

From Eq. (5), CHF fully accounts for the catalytic activity of $FeCl_3$ as a Lewis acid in xylan hydrolysis within an Arrhenius-type framework, as it also reflects the activation energy of the catalytic reaction. Among the contributing variables, $FeCl_3$ concentration serves as the most representative parameter, since the presence of hydronium ions generated by metal salts alone cannot fully characterize the Lewis acid behavior governing catalytic xylan hydrolysis (Chen and Lee, 2020; Kamireddy et al., 2013; Lu et al., 2025). The inclusion of $FeCl_3$ concentration, alongside temperature and time as operational variables, enables CHF, formulated as a modified severity factor, to reliably capture the combined effects of these parameters (Ji et al., 2017; Jiang et al., 2023). Consequently, CHF functions as a unified parameter for describing pretreatment severity in $FeCl_3$-catalyzed systems.

Xylan was divided into fast-hydrolysing X_f and slow-hydrolyzing X_s fractions. The hydrolysis rates for these fractions were described as the following Eq. (6) and (7) (Jiang et al., 2023; Ma et al., 2018; Zhu et al., 2012).

$$\frac{dX_f}{dt} = -kCX_f \tag{6}$$

$$\frac{dX_s}{dt} = -fkCX_s \tag{7}$$

where f is the ratio of the rate constants for slow and fast xylan hydrolysis. The initial proportion of slow-hydrolyzing xylan is denoted by θ. By solving these rate equations, the residual xylan content was expressed as a function of CHF, as shown in Eq. (8)

$$X_{res} = (1-\theta)\exp(-CHF) + \theta\exp(-fCHF) \tag{8}$$

By fitting this model to the experimental data, the constants α, β, E_a, θ, and f were determined, providing insights into the influence of pretreatment conditions, specifically temperature and $FeCl_3$ concentration on xylan solubilization and overall pretreatment efficiency. The objective function F_1 was minimized to optimize the fit between the modeled and experimental residual xylan values, as described below.

$$F_1 = \sum_{i=1}^{N}\left(X_{\mathrm{res},i}^{\mathrm{model}} - X_{\mathrm{res},i}^{\mathrm{exp}}\right)^2 \tag{9}$$

where N is number of data, $X_{\mathrm{res},i}^{\mathrm{model}}$ and $X_{\mathrm{res},i}^{\mathrm{exp}}$ are the modeled and experimental residual xylan.

Both fast- and slow-hydrolyzing xylan fractions are converted into xylose, denoted as X_x. As the xylose concentration increases, a simultaneous degradation reaction occurs, leading to the formation of byproducts such as furfural (du Pasquier et al., 2024; Wei et al., 2018). The mathematical representation of xylose formation and degradation, incorporating the correlation with CHF, is provided in Eq. (10)–(12).

$$\frac{dX_x}{dt} = kCX_f + fkCX_s - k_2CX_x \tag{10}$$

$$\frac{dX_x}{dt} = kC(1-\theta)X_0 exp(-kCt) + fkC\theta X_0 exp(-fkCt) - k_2CX_x \tag{11}$$

$$\frac{dX_x}{dt} + k_2CX_x = kC(1-\theta)X_0 exp(-kCt) + fkC\theta X_0 exp(-fkCt) \tag{12}$$

Solving this linear ODE yields Eq. (13).

$$X_x = \frac{kC}{k_2C - kC}(1-\theta)X_0(exp(-kCt) - exp(-k_2Ct)) + \frac{fkC}{k_2C - fkC}\theta X_0(exp(-fkCt) - exp(-k_2Ct)) \tag{13}$$

Rewriting using $CHF = kCt$ and define the ratio of $k_2/k = k_d$ as ratio of rate constant of xylose degradation and fast xylan hydrolysis process, and X_x/X_0 as xylose yield Y_x, it was obtained Eq. (14).

$$Y_x = \frac{(1-\theta)}{k_d - 1}\exp(-CHF) + \frac{\theta}{\frac{k_d}{f} - 1}\exp(-f \times CHF) - \left(\frac{(1-\theta)}{k_d - 1} + \frac{\theta}{\frac{k_d}{f} - 1}\right)\exp(-k_d \times CHF) \tag{14}$$

The objective function F_2 was minimized to optimize the fit between the modeled and experimental xylose yield values, as described below

$$F_2 = \sum_{i=1}^{N}\left(Y_{x,i}^{\mathrm{model}} - Y_{x,i}^{\mathrm{exp}}\right)^2 \tag{15}$$

where N is number of data, $Y_{x,i}^{\mathrm{model}}$ and $Y_{x,i}^{\mathrm{exp}}$ are the modeled and experimental xylose yield.

The objective functions, Eqs. (9) and (15) were minimized by MATLAB 2022a.

2.4. Enzymatic hydrolysis

The enzymatic hydrolysis of CCH was conducted using a cellulase enzyme, following the method outlined by (Huo et al., 2023). In this process, 0.5 g of solid residues, either raw or pretreated, were mixed with a buffer solution composed of citric acid and sodium citrate, adjusted to a pH of 4.8. The mixture was then supplemented with 20 FPU/g substrate. The reaction was carried out in a shaker incubator at 50 °C for 72 h, operating at a rotational speed of 150 rpm. The saccharification yield was determined using Eq. (16) (Tang et al., 2023).

$$\%Y_{EH} = \frac{released\ glucose \times 0.9_{(gram)}}{cellulose\ in\ substrate_{(gram)}} \times 100\% \tag{16}$$

where $\%Y_{EH}$ is the enzymatic hydrolysis yield from hydrolysate.

The improvement in enzymatic digestibility following pretreatment—attributed to xylan removal and increased cellulose accessibility, was represented by the correlation between CHF and enzymatic hydrolysis yield $\%Y_{EH}$, as described by the empirical relationship in Eq. (17) (Jiang et al., 2023; Zhu et al., 2012).

$$\%Y_{EH} = a \cdot exp(b \cdot CHF) + c \tag{17}$$

Eq. (17) was chosen to represent the relationship between $\%Y_{EH}$ and CHF, as it effectively models the characteristic exponential increase in hydrolysis efficiency with rising pretreatment severity. In this equation, a, b, and c serve as fitting parameters.

2.5. Analytical method

2.5.1. Determination of sugars in liquid hydrolysate and solid compositional analysis

The monomeric sugar content in hydrolysates from HTP, solid compositional hydrolysate, and enzymatic hydrolysis processes were analyzed using high-performance liquid chromatography (HPLC). A Thermo Scientific Vanquish Core HPLC system (Thermo Scientific, USA) equipped with a HyperREZ XP Carbohydrate Pb++ column (8 µm, 300

× 7.7 mm) and a refractive index (RI) detector was used for sugar analysis. The HPLC conditions were optimized with a flow rate of 0.6 mL/min, a column temperature of 85 °C, a system pressure of 9 bar, and HPLC-grade water as the mobile phase. Inhibitor compounds were analyzed using a Bio-Rad Aminex HPX-87H column with 5 mM H_2SO_4 as the mobile phase, at a flow rate of 0.6 mL/min and a column temperature of 50 °C. The inhibitors were expressed as follows.

$$\%Inhibitors = \frac{Inhibitor\ compound}{initial\ hemicellulose\ or\ cellulose} \times 100\% \quad (18)$$

In this study, the identified inhibitor compounds included furfural and acetic acid, derived from hemicellulosic sugar, as well as 5-hydroxymethylfurfural (5-HMF) and formic acid, derived from glucose (cellulose).

The compositional analysis of the biomass was conducted following the NREL method (Sluiter, 2008). This procedure involved hydrolyzing the biomass with concentrated sulfuric acid to quantify carbohydrate components, specifically monomeric sugars, and to determine the lignin content, including acid-soluble lignin (ASL) and acid-insoluble lignin (AIL).

The effect of HTP on the CCH biomass was evaluated by determining the recovery of solids and the removal of specific CCH components. These parameters were calculated using Eqs. (18) and (19).

$$Rec.Solids\ (\%) = \left(\frac{Pretreated\ CCH\ mass_{(g)}}{Initial\ CCH\ mass_{(g)}}\right) \times 100 \quad (19)$$

$$R_i(\%) = \left(1 - \frac{pretreated\ CCH\ component\ mass_{(g)}}{initial\ CCH\ component\ mass_{(g)}}\right) \times 100 \quad (20)$$

where R_i denotes the removal percentage of a specific CCH component i (hemicellulose, cellulose, or lignin).

2.5.2. Crystallinity, morphology, and functional group analyses of CCH

The influence of pretreatment variables on the crystallinity, morphology, and functional groups of CCH was also investigated. The crystallinity of solid fractions, both hydrothermally pretreated and untreated, was assessed using X-ray diffraction (XRD) following Segal's method (Sangadji et al., 2024). XRD measurements were performed using an X'Pert PRO (PAN-analytical BV, Netherlands) with Cu Kα radiation, operating at 40 kV and 30 mA. The crystallinity index (CrI) was determined using Eq. (20).

$$CrI\ (\%) = \frac{I_{002} - I_{am}}{I_{002}} \times 100\% \quad (21)$$

where I_{002} is the intensity of the 002 cellulose diffraction plane at 22.6°, and I_{am} is the intensity of the amorphous cellulose region at 18°.

Morphological changes in CCH after various pretreatments were observed using scanning electron microscopy (SEM) (Hitachi FlexSEM 1000, Japan). Additionally, Fourier transform infrared (FTIR) spectroscopy (Agilent Cary 630 FTIR Spectrometer, USA) was used to analyze changes in functional groups within the CCH samples.

Table 1
Fitting parameters of CCH xylan hydrolysis using Eq. (8)

Parameter	Unit	Value
θ	none	0.1721
α	none	22.17
β	L/mol	−3.38
E_a	J/mol	73,298
f	none	0.0422

3. Results and discussions

3.1. Xylan hydrolysis and CHF determination

This study investigated the kinetics of xylan hydrolysis using the CHF, which consolidates key reaction parameters, including time, temperature, and catalyst concentration. All fitting parameters in Eq. (8) were summarized in Table 1 and corresponding actual variables (temperature and $FeCl_3$ concentration) were listed in Table S2. The model, as fitted with Eq. (8), demonstrates a strong correlation between CHF and xylan dissolution, as indicated by a high R^2 value of 0.9801. The experimental data for residual xylan (X_{res}) were compared with predictions from a CHF-based kinetic model, as illustrated in Fig. 1a. Additionally, a parity plot (Fig. 1b) was used to evaluate the accuracy of the model in estimating residual xylan content across various CHF values. The parity plot (Fig. 1b) shows most data points closely aligned with the 1:1 line, confirming the model's predictive accuracy across the CHF range. This strong correlation reflects the model's capacity to integrate the combined effects of temperature, time, and $FeCl_3$ concentration into a single predictive parameter, the CHF. The minimal deviation observed suggests that CHF adequately captures the main kinetic trends associated with xylan hydrolysis under $FeCl_3$-HTP conditions. Compared to previous studies, the CHF parameter demonstrates a stronger correlation and greater utility than conventional severity factor (SF) or combined severity factor (CSF), which are often used merely to indicate pretreatment severity or serve as a general harshness index (Gao et al., 2023; Ilanidis et al., 2021; Kumar et al., 2019; Yang et al., 2023). Only a few studies have examined the predictive relationship between severity parameters and xylan hydrolysis, and those that did reported lower determination coefficients ($R^2 = 0.53–0.96$) compared to the present study using CHF (Abouelela et al., 2023; du Pasquier et al., 2024; Zhu et al., 2023). These findings highlight CHF as a powerful tool not only for integrating pretreatment conditions but also for accurately predicting xylan dissolution, an essential step in lignocellulosic biomass fractionation and valorization via hydrothermal pretreatment.

A rapid decline in residual xylan is observed at low CHF values (<6), suggesting that a majority of the xylan fraction is hydrolyzed under moderate pretreatment severity. Beyond this value, the residual xylan content stabilizes, indicating that primarily the recalcitrant, slow-hydrolyzing fraction remains. This behavior was also reflected in the fitting parameters θ and f, which were determined to be 0.1721 and 0.0422, respectively. The parameter θ represents the fraction of slow-hydrolyzing xylan that remains during severe pretreatment conditions, while f denotes the rate ratio between the slow and fast-hydrolyzing xylan fractions. This value corresponds to the slow-hydrolyzing fraction of xylan, which requires harsher reaction conditions for complete solubilization. This biphasic behavior reflects the nature of xylan distribution within the biomass cell wall. At low CHF, fast-hydrolyzing xylan, located in the outer layers of the cell wall or in regions not tightly associated with lignin or cellulose, is more readily hydrolyzed compared to slow-hydrolyzing xylan, which is more strongly embedded in the matrix, often in association with lignin and cellulose (Mittal et al., 2015). This trend has also been observed in dilute inorganic and organic acid pretreatments, where rapid xylan dissolution occurs at CHF values below 20, followed by the need for harsher conditions to further hydrolyze the remaining fraction (Jiang et al., 2023; Ma et al., 2018).

Another fitting parameter, activation energy (E_a) for xylan hydrolysis was determined to be 73,298 J/mol, which aligns with values reported for biomass and indicates a significant energy barrier associated with xylan depolymerization in CCH. This high value is attributable to the structural rigidity of the lignocellulosic matrix, where xylan is often cross-linked with lignin, requiring considerable activation energy for effective solubilization (Ji et al., 2017; Ruiz et al., 2021; Zhu et al., 2012). Additionally, the catalytic activity of $FeCl_3$ as a Lewis acid, capable of forming complexes and polarizing water molecules, also promoting the cleavage of glycosidic bond and contributes to the

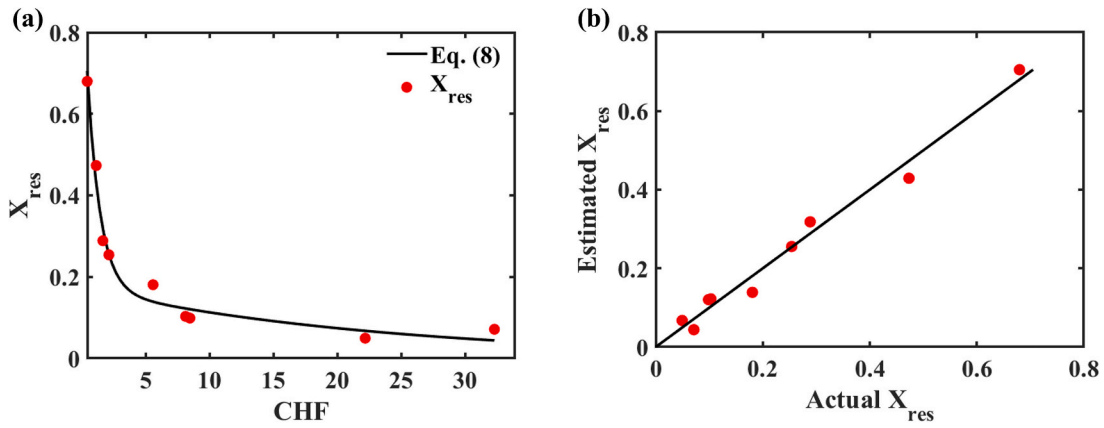

Fig. 1. (a) Correlation between CHF and residual xylan (X_{res}) fitted with Eq. (8), (b) parity plot between actual and estimated (X_{res}).

observed activation energy (Kamireddy et al., 2013). Other study has reported activation energies of 72,230 J/mol for densified corn stover pretreated with dilute sulfuric acid, where not only hydronium ions but also the densification process, which disrupts the lignocellulosic chemical structure, played a role in lowering the energy activation. In contrast, other study using organic acids, such as p-toluenesulfonic acid for the pretreatment of poplar, reported a considerably higher activation energy of 97,852 J/mol, suggesting that both biomass type and catalyst nature significantly influence the energy requirement (Ji et al., 2017). Comparatively, the activation energy observed in $FeCl_3$-assisted pretreatment is relatively low despite the absence of mechanical treatment, indicating that metal salt catalysts like $FeCl_3$ offer a lower activation energy alternative for xylan solubilization.

Lastly, these results demonstrate that CHF provides a strong predictive capability for xylan hydrolysis in $FeCl_3$-assisted pretreatment. The high correlation and robustness of the model are crucial for scaling up the process, as they offer valuable insights into the trade-offs among pretreatment variables and support the development of more efficient or alternative pretreatment strategies.

3.2. *Effect of $FeCl_3$-HTP conditions on components removal and compositional change*

The effect of CHF, representing pretreatment conditions during $FeCl_3$-catalyzed hydrothermal pretreatment (HTP), on the removal of CCH components is shown in Fig. 2. The fitted CHF values calculated from Eq. (8) are presented on the lower horizontal axis, while the corresponding pretreatment temperatures (120–180 °C) and $FeCl_3$ concentrations (20–100 mM) are displayed on the upper horizontal axis. Fig. 2a illustrates the relationship between CHF and the removal of major CCH components, along with the percentage of recovered solids after pretreatment. The solid recovery decreased from 88.23 % and stabilized around 48.07-54.2 % as the temperature and $FeCl_3$ concentration increased from 120 °C and 20 mM to 180 °C and 100 mM, respectively. This trend indicates the progressive dissolution of CCH components, including hemicellulose, cellulose, and lignin. As pretreatment severity increased, represented by higher CHF values, each biomass component was progressively degraded to varying extents (Ma et al., 2021; Yao et al., 2021).

As CHF increased, the removal of hemicellulose (R_H) was the most prominent compared to other components. R_H rose sharply from 32.03 % to 89.7 % as CHF increased from 0.43 to 8.13 and then stabilized between 90.12 % and 95.05 % as removal approached completion at CHF 32.28. This behavior is consistent with the xylan hydrolysis trend observed in Fig. 1a. In contrast, cellulose removal (R_C) increased more gradually, from 7 % to 30.1 % between CHF 0.43 and 8.46, and exhibited a more significant rise under harsher conditions, reaching 57.3–67.4 % at higher CHF values. These results indicate that $FeCl_3$-HTP is highly selective and effective for hydrolyzing hemicellulose at mild to moderate conditions. Similar phenomena have been reported previously (Wu et al., 2018), where increasing pretreatment severity led to hemicellulose (represented by xylan) and cellulose removal of 75.6–85.8 % and 6.2–18 %, respectively. These findings further confirm that hemicellulose is far more susceptible to hydrothermal degradation and can be selectively removed during $FeCl_3$-HTP (Wu et al., 2018; Zhang et al., 2020). The selective behavior observed in these results could be attributed to the amorphous nature of hemicellulose, its low degree of polymerization, and its more exposed location within the biomass structure compared to cellulose (Tang et al., 2021; Xiao et al., 2013). These characteristics make hemicellulose more susceptible to hydrolysis by $FeCl_3$, with hydrolysis further enhanced as the catalyst concentration increases. Additionally, elevated temperatures contribute to the disruption of the hemicellulose structure, accelerating its hydrolysis. The low degree of polymerization and heteropolymeric structure of hemicellulose result in fewer intra-molecular hydrogen bonds, making it inherently more vulnerable to chemical degradation (Saini et al., 2024). In contrast, cellulose has a degree of polymerization approximately 100 times higher than hemicellulose and is stabilized by extensive intra- and inter-molecular hydrogen bonding, facilitated by its β-1,4-glycosidic linkages. This gives cellulose a highly crystalline structure, rendering it significantly more resistant to hydrolysis under similar pretreatment conditions (Li et al., 2017; Xiao et al., 2013). The phenomenon of selective hemicellulose removal has also been observed in $FeCl_3$-catalyzed pretreatment of rapeseed straw and waste wheat straw, where hemicellulose removal reached 92.6 % and 97.2 %, respectively, while cellulose and lignin removal remained relatively low (Romero et al., 2018; Tang et al., 2021).

The removal of the third major component, lignin (R_L), was the lowest among all biomass fractions. As CHF increased, no abrupt rise in R_L was observed; lignin removal ranged only from 2.6 % to 11.9 % between CHF 0.43 and 8.46. Under harsher conditions (CHF 22.18–32.28), R_L showed a slight decrease and subsequently stabilized. This behavior can be attributed to the inherent structural characteristics of lignin, which include a highly cross-linked aromatic network, hydrophobicity, and high molecular weight, making the ether bonds in lignin significantly more resistant to cleavage by hydronium ions generated from the Fe^{3+}-water complex, compared to the glycosidic bonds in cellulose and hemicellulose (Kumar et al., 2009). At severe pretreatment conditions, lignin may undergo condensation reactions, leading to increased structural stability. Additionally, the formation of pseudolignin, arising from sugar degradation products that repolymerize into lignin-like structures, may contribute to the slight bias observed in R_L values at high CHF (Mu et al., 2019; Wan et al., 2019). Similar phenomena have been reported (Tang et al., 2022, 2021), where lignin removal ranged only from 27.2 % to 35.2 % at 180 °C and 20–100 mM $FeCl_3$, significantly lower compared to the removal of hemicellulose

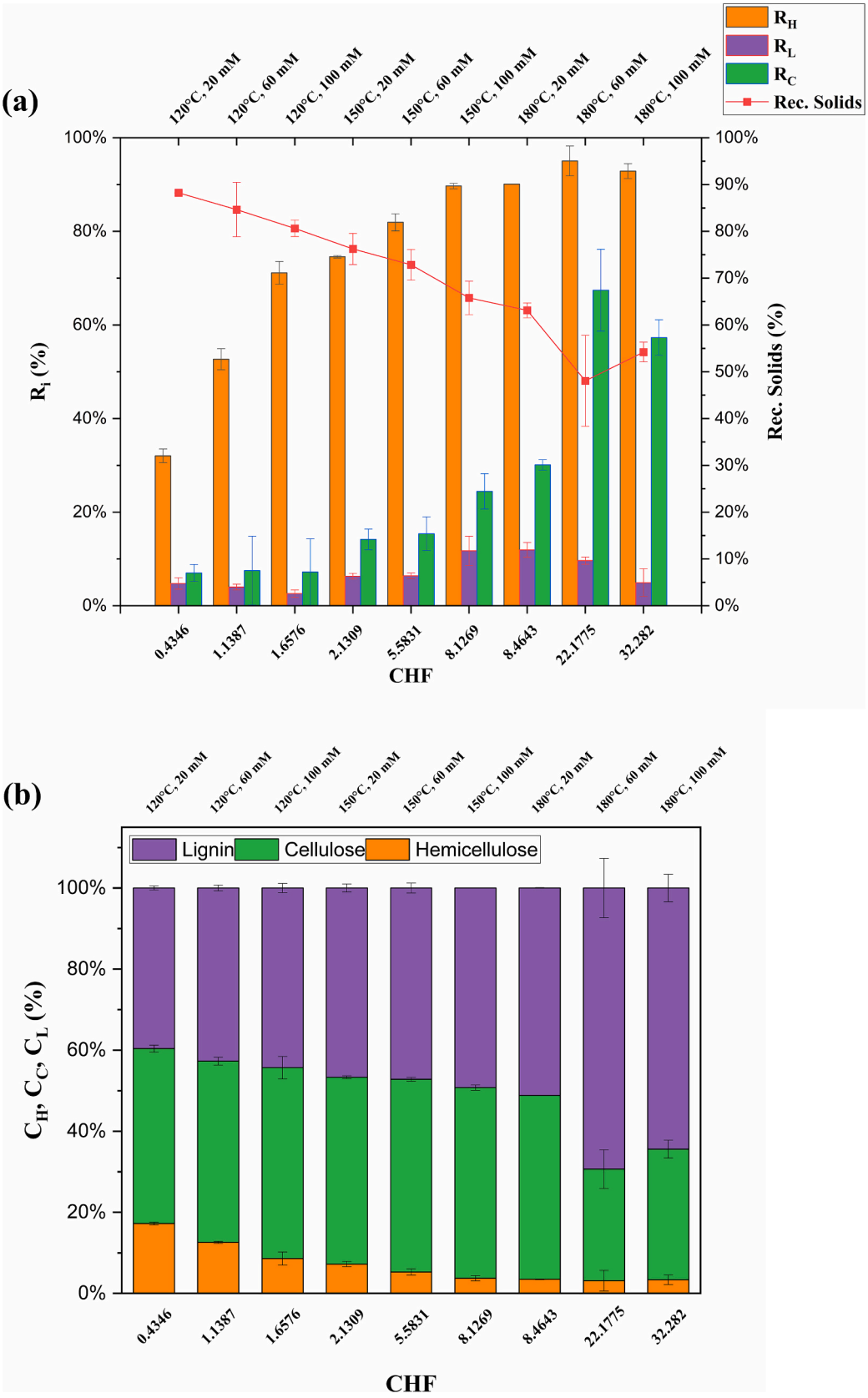

Fig. 2. Effect of $FeCl_3$-HTP on CCH components removal (a) and relative compositions (b)

and cellulose (represented by xylan and glucan). Moreover, lignin removal tended to stabilize at higher $FeCl_3$ concentrations (80–100 mM) due to the formation of condensed lignin. However, the lignin removal observed in this study was even lower than previous reports (Tang et al., 2022, 2021; Wu et al., 2018), where waste wheat straw showed lignin removal up to 33.7 % at 20 mM $FeCl_3$, 180 °C, and 40 min. This indicates that the lignin in CCH is more recalcitrant compared to other biomasses, likely due to its inherently higher lignin content. The high residual lignin remaining after $FeCl_3$-HTP suggests a promising opportunity for lignin valorization through suitable extraction methods, enhancing the overall efficiency and economic viability of CCH fractionation and biorefinery processes.

The removal of the three main biomass components during $FeCl_3$-HTP significantly influenced the composition of pretreated CCH, as shown in Fig. 2b. As captured by the CHF parameter, the high hemicellulose removal (R_H) resulted in a substantial decrease in hemicellulose content—from 17.22 % in raw CCH to just 3.14 % at CHF 5.58, indicating near-complete elimination of this fraction. Consequently, the relative proportions of remaining compounds, particularly cellulose, increased from 38.0 % in raw CCH to 47.6 % in pretreated CCH at CHF 5.58. This enrichment is beneficial for downstream processes, such as enzymatic hydrolysis, as it not only increases cellulose availability but also enhances its exposure, thereby improving digestibility. These results are consistent with previous studies, where $FeCl_3$-HTP achieved near-complete hemicellulose removal, leaving only 2.15 % hemicellulose in pretreated sugarcane bagasse, while cellulose and lignin remained as the dominant solid components (Chen et al., 2014; Romero et al., 2018; Tang et al., 2022). However, at CHF values above 8.46, further increase in pretreatment severity led to excessive cellulose exposure and subsequent degradation. As a result, cellulose removal (R_C) increased, reducing the cellulose content in the pretreated solids, while the relative lignin content continued to rise. This suggests that under harsh conditions, the selectivity of $FeCl_3$-HTP diminishes, leading to the breakdown of both hemicellulose and cellulose. A similar trend was reported in the pretreatment of olive tree biomass, where increasing the temperature from 160 °C to 180 °C and $FeCl_3$ concentration from 0.2 to 0.275 M resulted in a substantial cellulose loss from 50 % to 88.2 % (López-Linares et al., 2013).

Overall, CHF, as an integrated parameter representing pretreatment conditions during HTP, successfully captured the behavior of component removal and changes in lignocellulosic composition. These results demonstrate that CHF is an effective tool for describing the trends in component solubilization under $FeCl_3$-catalyzed HTP. Furthermore, the use of CHF is beneficial for process scale-up, providing a practical means to predict biomass fractionation behavior. This finding also suggests that further optimization studies using CHF in $FeCl_3$-HTP could enhance the selective separation of lignocellulosic components during biomass pretreatment.

3.3. *Effect of $FeCl_3$-HTP conditions on hemicellulosic sugar yield and degradation products*

Fig. 3 illustrates the trend of hemicellulosic and glucose sugar yield (Y_{HS}) meanwhile degradation products formation as a function of CHF during $FeCl_3$-HTP. The yield includes sugars such as xylose, galactose, arabinose, and mannose, highlighting their dependence on pretreatment severity. Among these, xylose is the most dominant, accounting for up to 89 % of the total hemicellulosic sugars. This is expected, as xylose is the primary backbone monomer of hemicellulose, while the other sugars typically occur as side chains in the hemicellulose structure (Curry et al., 2023; Kaur et al., 2024). At low CHF values (0.43–1.14) of Fig. 3a, the hemicellulosic sugar yield (Y_{HS}) remains relatively low, ranging from 10.3 % to 41.3 %. These mild pretreatment conditions, corresponding to temperatures of 120 °C and $FeCl_3$ concentrations of 20–60 mM, result in limited hemicellulose hydrolysis and minimal sugar release. As CHF increases to the range of 1.66–5.58 (120 °C with 100 mM $FeCl_3$ and 150 °C with 60 mM $FeCl_3$), Y_{HS} increased significantly, peaking at 64 % under the latter condition. This trend is consistent with the increased hemicellulose removal observed at moderate pretreatment severity, as discussed previously. The enhanced sugar release can be attributed to both the thermal effect and the catalytic activity of $FeCl_3$. Fe^{3+} ions form hydration spheres through covalent coordination with water molecules, creating a polarized environment that increases the concentration of reactive hydronium ions (Esmaeilbeig et al., 2022; Kamireddy et al., 2013). These hydronium ions effectively catalyze the hydrolysis of glycosidic bonds in hemicellulose, particularly xylan, leading to the release of xylose and other hemicellulosic sugars (Li et al., 2022; Tang et al., 2021). This catalytic mechanism differs from that of conventional inorganic acid pretreatment, where catalytic strength is primarily governed by solution pH (Zhao et al., 2023). Therefore, the use of a modified CHF is appropriate to capture the catalytic behavior of $FeCl_3$, as it accounts for catalyst concentration in addition to thermal effects, rather than relying solely on pH. Meanwhile, beyond CHF 5.58, the hemicellulosic sugar yield begins to decline sharply, eventually reaching very low levels. This indicates sugar degradation or the formation of inhibitory by-products under severe pretreatment conditions.

Fig. 3a also illustrates glucose release, represented as glucose yield (Y_G), which reflects cellulose degradation during $FeCl_3$-HTP. As CHF increased, glucose yield rose from 0.5 % to a maximum of 13.6 %. In contrast to hemicellulosic sugars, glucose release remained relatively low, consistent with the limited cellulose removal discussed earlier. This behavior is attributed to the highly ordered, crystalline structure of cellulose, which is stabilized by extensive intra- and intermolecular hydrogen bonding, making it more resistant to hydrolysis during hydrothermal pretreatment (Sun et al., 2021). However, at the highest CHF tested in this study (32.28), glucose yield also declined, likely due to degradation of glucose into by-products such as 5-hydroxymethylfurfural (5-HMF) under severe conditions (Ma et al., 2021).

In parallel with the decline in sugar yield, Fig. 3b presents the trend of degradation products (inhibitors) as a function of CHF. Across the range CHF 0.43–32.3, inhibitor concentrations increased progressively, varying from 3.06 to 16.9 % for furfural, 1.82–16 % for acetic acid, 0.66–7.89 % for 5-HMF, and 0.42–4.67 % for formic acid. Among these, 5-HMF and formic acid exhibited gradual increases over the entire CHF range, consistent with their formation via glucose dehydration. In contrast, furfural and acetic acid displayed two distinct phases, a moderate increase from CHF 0.43–5.58, followed by a sharp rise at higher severities up to CHF 32.3. This shift corresponds to the rapid decline in xylose yield beyond CHF 5.58, attributable to the dehydration of released xylose into furfural under harsher conditions (Gao et al., 2023; Huang et al., 2019). Furfural and acetic acid were the dominant inhibitors, confirming the predominance of hemicellulose degradation during $FeCl_3$-catalyzed HTP. As CHF increased, harsher reaction conditions favored the formation of these degradation products, indicating that $FeCl_3$ catalysis not only promotes hemicellulose removal but also accelerates inhibitor generation at elevated severities. Similar trends have been reported in previous studies. (Gao et al., 2023) observed that xylose yield from corncob hydrolysis increased from 4.4 % to 61.3 % as temperature rose from 140 °C to 160 °C and $FeCl_3$ concentration from 0 to 50 mM but subsequently declined at 180 °C and 100 mM $FeCl_3$ due to sugar degradation. Likewise, others reported that in $FeCl_3$ pretreatment of wheat straw, higher severities decreased xylose yield while increasing formic acid, acetic acid, furfural, and 5-HMF concentrations (Tang et al., 2021).

These inhibitors can cause significant challenges in downstream fermentation. In this study, measured concentrations ranged from 0.38 to 2.09 g/L for furfural and 0.13–1.51 g/L for 5-HMF based in Fig. 3b. Based on these values, the total furan concentration (furfural +5-HMF) is predicted to exceed the reported critical threshold of 2.5 g/L when CHF > 8.13 (150 °C, 0.1 M $FeCl_3$). Previous reports indicate that this total furan level can reduce ethanol production rates by an order of magnitude during fermentation (Millán Acosta et al., 2021). Beyond this

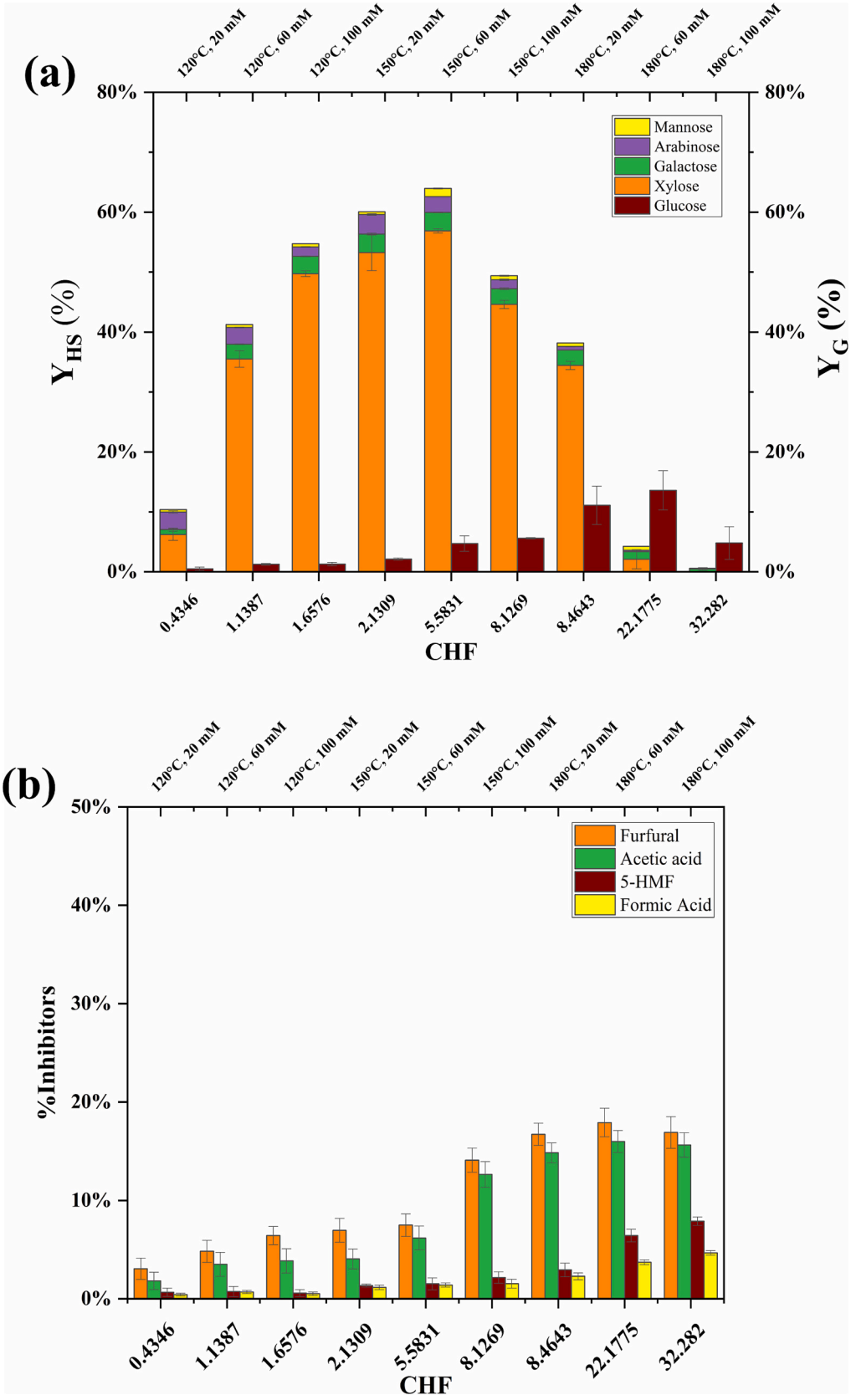

Fig. 3. $FeCl_3$-HTP effect on (a) hemicellulosic and glucose sugar yield of CCH, meanwhile (b) degradation products

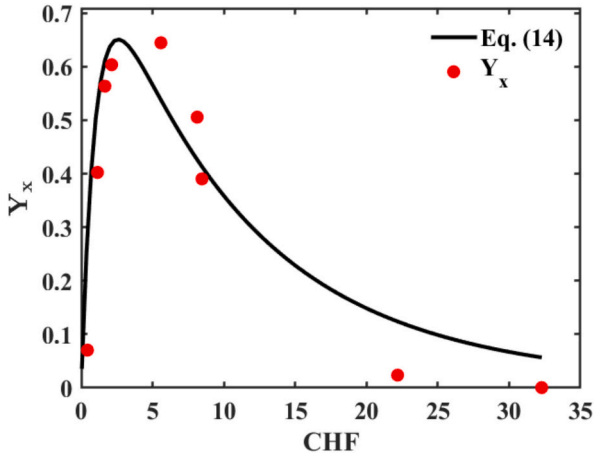

Fig. 4. Xylose yield and CHF correlation

severity, the fermentation process becomes less economically feasible due to the combined effects of high inhibitor concentrations and the increased energy input required for HTP. Therefore, maximizing sugar yield while maintaining low furan concentrations is essential for process viability. If complete avoidance of high furan levels is not possible, detoxification strategies should be employed to enhance bioethanol production. Potential approaches include chemical detoxification, improving microbial tolerance to inhibitors, or co-culturing with detoxifying fungal strains capable of processing hydrolysates containing up to 6 g/L total furans without compromising ethanol yield (C. Liu et al., 2024a; Liu et al., 2019; Millán Acosta et al., 2021; Shah et al., 2025). Future studies should evaluate the trade-off between maximizing biofuel yield and the cost of detoxification, ensuring an optimal balance between pretreatment efficiency and downstream fermentation performance (Bhatia et al., 2020; Ilanidis et al., 2021; Leal Silva et al., 2022).

The result of Y_{HS} and Y_G in response of pretreatment variables or by CHF parameter were showing the behavior of peak yield which open the further investigation in order to maximize the total recovered sugar during $FeCl_3$-HTP. This important result significantly elucidates the behavior of the pretreatment process for scale-up applications, as CHF can be reliably used as a unifying parameter to describe the trade-offs among pretreatment conditions in relation to sugar recovery.

The previous discussion motivated a kinetic study of xylose production, based on the biphasic behavior of xylan dissolution. The resulting xylose yield (Y_X) was correlated with CHF, as shown in Fig. 4, achieving a determination coefficient (R^2) of 0.8131 and a fitted degradation constant (k_d) of 0.1051. The model describes the experimental and predicted xylose yields as a function of CHF, accounting for the kinetics of both fast- and slow-hydrolyzing xylan fractions, as well as xylose degradation (Jiang et al., 2023). The first two terms in Eq. (14), driven by exponential functions of CHF, represent the hydrolysis of fast- and slow-reacting xylan fractions, respectively. At low CHF values, a sharp increase in xylose yield is predicted due to the rapid hydrolysis of easily accessible xylan. As CHF increases, the slow-hydrolyzing xylan fraction becomes more dominant, resulting in a slower but continued rise in xylose yield, requiring higher pretreatment severity for effective breakdown. The model predicts a peak in xylose yield around CHF 4–5, where both xylan fractions have been substantially converted. Beyond this point, the third term in the model accounts for xylose degradation into by-products such as furfural, causing the yield to decline at higher CHF values. Furthermore, subsequent decline at higher CHF, supporting the model's predictive capability (Labauze and Benjelloun-Mlayah, 2021). While the R^2 value of 0.8131 indicates a reasonable fit, explaining over 81 % of the data variance, discrepancies at higher CHF values suggest that factors such as unaccounted xylo-oligosaccharides may contribute to the observed deviations. These oligomers may represent intermediate products in xylan hydrolysis that are not fully accounted for by the current model. Further refinement, incorporating the dynamics of xylo-oligosaccharide formation and additional pretreatment variables within the CHF framework could enhance the model's predictive accuracy. Other studies have empirically modeled xylose yield using the CSF, such as in the dilute acid pretreatment of poplar wood, which achieved an R^2 of 0.9065 (du Pasquier et al., 2024). While this fit is slightly higher than that obtained in the present study, the empirical equation used lacks the capacity to mechanistically describe hemicellulose solubilization and xylose degradation. In contrast, Eq. (14) in this study is theoretically derived to reflect the kinetics of xylan conversion and xylose degradation as a function of CHF, maintaining physical relevance. Thus, the continued development and application of CHF as a parameter to predict xylose yield remains both meaningful and advantageous. The CHF-based kinetic model presented here offers not only predictive capability but also a unified framework for consolidating pretreatment conditions while preserving the mechanistic interpretation of the process. This underscores its value as a tool for optimizing $FeCl_3$-HTP and other hydrothermal fractionation strategies.

3.4. Solid characterization of $FeCl_3$-HTP CCH

Fig. S1 (see supplementary data) presents the XRD analysis of $FeCl_3$-HTP-treated CCH, illustrating the impact of pretreatment conditions as represented by the CHF. The XRD pattern of CCH displayed characteristic peaks of cellulose, with two major reflections observed at $2\theta \approx 18^\circ$ and 22.6°, corresponding to the amorpous peak and (002) crystal planes, respectively. The crystallinity index (CrI) increased from 63.3 % in the untreated sample to a peak of 78.6 % at CHF 8.1, indicating that pretreatment effectively removed amorphous components, primarily hemicellulose and, to a lesser extent, lignin, thereby enhancing the relative visibility of the crystalline cellulose structure. This trend is consistent with the component removal data shown in Fig. 2, where increasing CHF led to higher removal of non-cellulosic fractions and a corresponding increase in cellulose content in the pretreated CCH (Yao et al., 2021). However, at higher CHF values (8.4 to 32.26), a decline in CrI was observed, suggesting that under harsher conditions, cellulose crystallinity began to degrade. The elevated temperatures and higher $FeCl_3$ concentrations likely disrupted intra- and intermolecular hydrogen bonding and facilitated partial hydrolysis of cellulose, leading to a loss of crystalline integrity (Kumar et al., 2019; Sun et al., 2021). As a result, the reduction in CrI at severe conditions may enhance the accessibility of enzymes by exposing more amorphous cellulose regions, which can be more readily hydrolyzed to glucose (Gao et al., 2025). Similar phenomena have been reported in other studies. For example, an increase in cellulose concentration was accompanied by an increase in CrI (Tang et al., 2022), and CHF has been shown to influence cellulose enrichment and crystallinity in pretreated biomass (Ji et al., 2017) Conversely, under more severe pretreatment conditions, a decrease in CrI has also been observed due to cellulose degradation (Yao et al., 2021).

The morphology of CCH (Fig. S2, see supplementary data) at each pretreatment temperature with 60 mM $FeCl_3$ was analyzed to evaluate the impact of $FeCl_3$-HTP on structural integrity. The untreated raw CCH exhibited a smooth and compact surface, characteristic of an intact lignocellulosic matrix. Following treatment at 120 °C, the surface began to degrade and appeared rougher, indicating the initial disruption of hemicellulose, cellulose, and lignin. At 150 °C, the fiber structure became more open and disordered, and at 180 °C, the surface displayed pronounced roughness and fragmentation. In addition, irregular spherical or droplet-like deposits were observed on the fiber surfaces under the most severe conditions, similar to those reported in dilute acid- and metal salt-catalyzed hydrothermal systems (Shen et al., 2016; Wan et al., 2019). These droplets are typically attributed to recondensed lignin or pseudo-lignin formed from carbohydrate degradation products that

repolymerize and redeposit onto the biomass surface. While moderate droplet formation may correlate with lignin redistribution and increased fiber exposure, excessive coverage can physically block enzyme binding sites, potentially reducing digestibility despite increased porosity. These changes reflect progressive degradation of the lignocellulosic architecture with increasing pretreatment severity or CHF (Zhu et al., 2023) and illustrate the dual role of lignin-derived deposits in altering enzyme accessibility. This structural disruption enhances enzyme accessibility, which may contribute to improved cellulose conversion during enzymatic hydrolysis (Li et al., 2021).

Functional group analysis of pretreated CCH was conducted using FTIR spectroscopy, as shown in Fig. S3 and Table S1 (see supplementary data). The FTIR spectra can be broadly divided into two main absorption regions: the low wavenumber region (1030–1729 cm^{-1}) and the high wavenumber region (2907–3333 cm^{-1}). With increasing CHF, a decrease in absorbance at 3333 cm^{-1} and 2907 cm^{-1} was observed, corresponding to the O—H and C—H stretching vibrations, respectively. These functional groups are associated with hydroxyl groups in cellulose, hemicellulose, and lignin, as well as methyl and methylene groups in carbohydrates and lignin (Wu et al., 2019). The reduction in these peaks with increasing CHF suggests disruption of hydrogen bonding and partial degradation of carbohydrates, particularly hemicellulose and cellulose, consistent with the compositional changes discussed in Fig. 2. In the lower wavenumber region, peaks at 1729, 1371, 1327, and 1238 cm^{-1}, attributed to C═O stretching, O—H bending, and C—O bending, were also reduced or nearly disappeared at high CHF. These bands are characteristic of carbonyl groups in acetyl or ester functionalities and ether linkages in hemicellulose, indicating extensive hemicellulose removal under severe pretreatment conditions (Wang et al., 2021). In contrast, lignin-related peaks at 1603 cm^{-1} and 1509 cm^{-1}, representing aromatic C═C stretching and aromatic skeletal vibrations, respectively, remained visible as CHF increased (Gundupalli et al., 2022). Interestingly, these peaks became more intense at high CHF, suggesting an increase in lignin content in the solid residue. Similar FTIR trends have been reported in studies where severe pretreatment conditions promoted lignin condensation or pseudo-lignin formation, leading to an enrichment of aromatic structures in the pretreated solids (Shen et al., 2016; Wan et al., 2019). This observation aligns with the compositional analysis, confirming that the relative lignin proportion increases as hemicellulose and cellulose are progressively removed under harsh $FeCl_3$-HTP conditions, while lignin-derived condensation products may contribute to the enhanced aromatic signal. Overall, these FTIR results illustrate that the impact of $FeCl_3$-HTP on CCH is well described by the CHF parameter, which effectively captures the severity of pretreatment. Furthermore, the FTIR findings corroborate the results of the compositional analysis of pretreated CCH.

3.5. Enzymatic hydrolysis evaluation of pretreated CCH using CHF

As previously discussed, $FeCl_3$-HTP resulted in extensive removal of xylan (hemicellulose) from CCH, often approaching complete solubilization, while leaving cellulose largely intact but more structurally disrupted. This increased exposure and alteration of cellulose morphology, as confirmed by solid-state characterization, is likely to enhance enzymatic digestibility (Chen et al., 2015; Su et al., 2023). Therefore, CHF, which is derived from the pretreatment conditions and fitted to xylan hydrolysis behavior, can serve as a representative parameter for the state of pretreated CCH (Jiang et al., 2023; Zhu et al., 2012). As a result, CHF can be empirically correlated with enzymatic hydrolysis yield Y_{EH} as expressed in Eq. (17).

Fig. 5 shows the relationship between enzymatic hydrolysis yield Y_{EH} and CHF, fitted according to Eq. (17). The model successfully captured this correlation, achieving a high determination coefficient (R^2 = 0.9833), with the corresponding fitting parameters listed in Table 2.

Table 2
Eq. (17) fitting parameters and determination coefficients

Parameters	Value
a	−48.8206
b	−0.0236
c	61.9905
R^2	0.9833

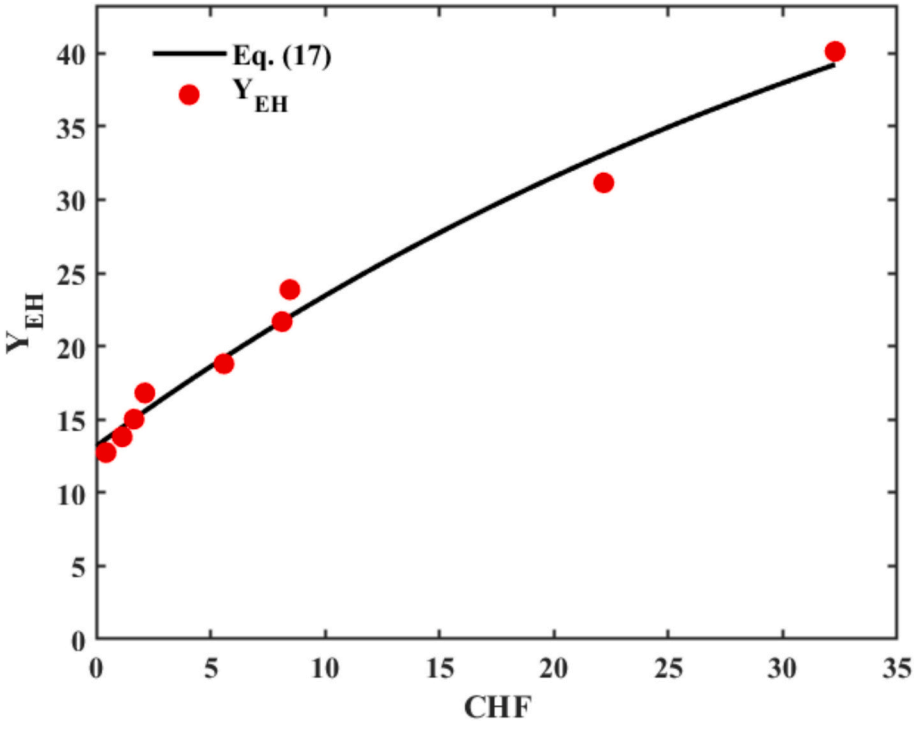

Fig. 5. CHF effect on enzymatic hydrolysis yield (Y_{EH})

This model is useful for predicting Y_{EH} of pretreated CCH based on CHF, demonstrating how pretreatment severity influences enzymatic digestibility. The increase in CHF was closely followed by a corresponding increase in Y_{EH}, indicating that xylan hydrolysis, and thus hemicellulose removal, plays a critical role in enhancing enzymatic digestibility (Tan et al., 2020). The concurrent increase in FTIR aromatic peak intensities at high CHF further suggests that, alongside hemicellulose removal, lignin condensation or pseudo-lignin formation alters the chemical environment of the cellulose surface. Depending on the extent of this redeposition, it may either have minimal impact or introduce localized resistance to enzymatic attack. This is strongly supported by earlier XRD, SEM, and FTIR analyses, which revealed extensive hemicellulose removal, disruption of cellulose crystallinity, increased surface roughness, and loss of hemicellulose-specific functional groups. These changes collectively improve cellulose accessibility to enzymes (Su et al., 2023; Tan et al., 2020).

This trend aligns with findings from other studies, which also reported increasing enzymatic digestibility with rising CHF as a result of more effective pretreatment and enhanced cellulose exposure (Ji et al., 2017; Jiang et al., 2023; Zhu et al., 2012). However, unlike some prior studies that identified a plateau region at high CHF, this study did not exhibit a stable phase, suggesting that Y_{EH} may continue to increase with CHF under the tested conditions. Nevertheless, as previously discussed, excessively high CHF can lead to significant cellulose degradation once hemicellulose is nearly completely removed, exposing cellulose and lignin to further chemical attack. Therefore, while CHF proves to be a reliable parameter for representing $FeCl_3$-HTP conditions and predicting enzymatic conversion, careful optimization is necessary to balance sugar recovery and cellulose preservation (Ruiz et al., 2023). These findings reinforce the value of CHF as a practical and scalable tool for designing efficient biomass pretreatment processes (Ruiz et al., 2020).

3.6. *Applicability of CHF parameter in describing another biomass pretreatment*

With identical pretreatment conditions and experimental design, the applicability of CHF as a unified parameter for describing pretreatment effects was further evaluated using oil palm empty fruit bunch (OPEFB) as a representative biomass. Fig. 6 compares the residual xylan, xylose yield, and enzymatic hydrolysis yield of CCH and OPEFB across the CHF range. The corresponding fitting parameters for OPEFB, obtained from Eqs. (8), (14), and (17), are summarized in Table S3, while corresponding CHF and actual variables values for each biomass are provided in Table S2. As shown in Fig. 6a, OPEFB exhibits a biphasic hydrolysis profile similar to that of CCH, with an initial rapid decline in residual xylan at low CHF values, followed by a slower reduction once the residual xylan fraction reaches a low concentration. This transition occurs at approximately CHF < 6 for the hydrolysis of fast-hydrolyzing xylan and CHF > 6 for the hydrolysis of the slow-hydrolyzing fraction. In parallel, the xylose yield of OPEFB increases with CHF, peaking in the range CHF = 2–5, consistent with the peak observed for CCH. Notably, the predicted maximum xylose yield for OPEFB is slightly higher than that of CCH, indicating that applying the same reaction system to different biomass types can yield similar CHF-dependent behavior, namely, a rapid drop in residual xylan followed by a xylose yield peak. This behavior is well captured by the CHF approach and is advantageous for the design of $FeCl_3$-catalyzed HTP reactors (Ruiz et al., 2021, 2020). The fitted constants in Table S3 reveal slight variations between the two biomasses, attributable to their intrinsic physicochemical properties under the $FeCl_3$ catalytic system. The higher activation energy (E_a) observed for CCH (73,298 J/mol) compared to OPEFB (71,451 J/mol) indicates that xylan hydrolysis proceeds more slowly in CCH, reflecting the greater energy barrier required to deconstruct xylan. This difference can be linked to initial composition, as CCH contains a higher lignin content (36.9 %) than OPEFB (32 %), contributing to a more recalcitrant lignin–xylan network via lignin–carbohydrate complexes (LCCs) availability that resist hydrolysis during HTP (Geng et al., 2019; Giummarella and Lawoko, 2017). This is consistent with the higher slow-hydrolyzing xylan fraction (θ) observed in CCH (0.1721) compared to OPEFB (0.1664). Such findings highlight the importance of characterizing lignocellulosic properties prior to pretreatment and correlating kinetic parameters with structural features. For example, woody biomasses such as Douglas fir, lodgepole pine, aspen, and poplar exhibit activation energies in the range 97,852–100,000 J/mol, and biomasses within the same class and catalytic system under dilute acid conditions often display comparable hydrolysis behavior and kinetic parameters (Ji et al., 2017; Zhang et al., 2014; Zhou et al., 2013; Zhu et al., 2012). In contrast, under different catalytic systems, including hydrotropic agents, dilute acids, densification combined with sulfuric acid, and also this study, these constants can vary widely, as evidenced by reported activation energies spanning 71,451–100,000 J/mol (Ji et al., 2017; Jiang et al., 2023; Ma et al., 2018; Zhang et al., 2014). This variation reflects the dominant influence of catalyst type as a controlling factor in pretreatment efficiency. Consequently, the transferability of kinetic constants for predicting xylan hydrolysis is feasible for biomass types of similar composition under the same catalytic system, but caution is warranted when applying them across systems with different catalytic chemistries.

While the CHF-based model captured xylan hydrolysis with high

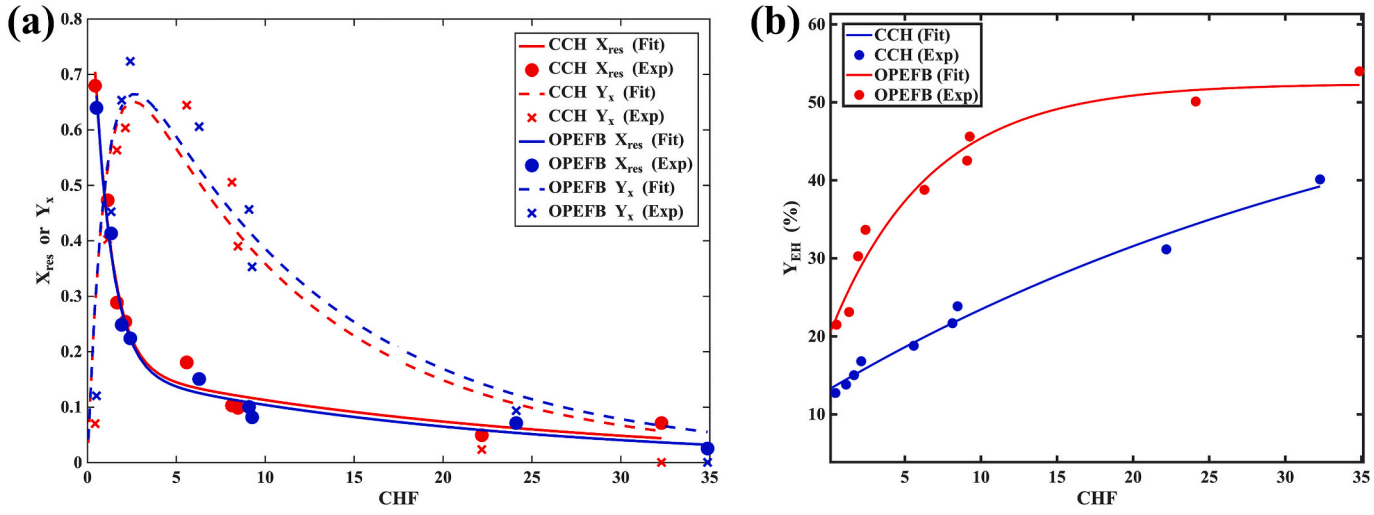

Fig. 6. CHF effects on residual xylan, xylose yield (a) and enzymatic hydrolysis yield (b) of CCH and OPEFB biomasses

accuracy, the correlation between xylose yield and CHF showed higher deviation than xylan hydrolysis. This is likely due to the model's simplifying assumption that all hydrolyzed xylan is directly converted to xylose, without accounting for oligomeric sugar before xylose and parallel degradation pathways leading to byproducts, which can become more significant at higher CHF values (Kaur et al., 2024; Shen et al., 2021; Warren-Walker et al., 2024). As a result, the determination coefficients (R^2) for the xylose yield model were lower, 0.8131 for CCH and 0.8588 for OPEFB, compared to the residual xylan model. Since this represents the first attempt to model xylose hydrolysis using the modified severity factor CHF, there remains scope for improvement. Future research should focus on refining the model to incorporate, oligomeric form of sugar, degradation product formation, and validating its applicability across a wider range of biomass types, including woody and other agricultural residues, to establish CHF as a more universally robust predictive parameter.

The effect of pretreatment severity on the enzymatic hydrolysis of cellulose for both pretreated biomasses is shown in Fig. 6b. In both cases, enzymatic hydrolysis yield increased with CHF, in parallel with hemicellulose removal. However, OPEFB consistently achieved higher enzymatic hydrolysis yields than CCH, suggesting that the lower recalcitrance of OPEFB facilitates greater cellulose accessibility following pretreatment. This difference underscores that while CHF serves as a robust unified parameter for describing pretreatment effects, biomass-specific structural features, such as cellulose crystallinity, degree of polymerization, non-cellulosic components, and other microstructural attributes, continue to influence the ultimate digestibility of pretreated cellulose. These factors also affect the residual composition of biomass, which can contribute to non-productive enzyme binding and limit hydrolysis efficiency (Jia et al., 2021; Shi et al., 2025; Su et al., 2023).

These findings demonstrate the applicability of the CHF parameter to different biomass types and its effectiveness in guiding reactor design and scale-up for $FeCl_3$-catalyzed HTP when the target is xylan hydrolysis, as evidenced by the consistent behavior observed across biomasses under the same catalytic system. Further investigation is warranted to assess the influence of CHF on xylose formation and the enzymatic hydrolysis of cellulose from various pretreated biomasses. Such studies would strengthen the applicability of CHF in predicting downstream outcomes, including enzymatic digestibility and xylose production, thereby extending its utility beyond pretreatment optimization to the broader bioconversion process.

3.7. Process mass balance analysis of HTP-$FeCl_3$

The fractionation performance of $FeCl_3$-assisted HTP, coupled with enzymatic hydrolysis, was evaluated to determine the total recovered sugar from CCH. Fig. 7 compared raw CCH with HTP CCH through the mass balance analysis based on 100 g of raw CCH. Total sugar recovery increased from 7.4 g/100 g CCH at CHF 0.44 to a maximum of 22.04 g/100 g CCH at CHF 5.58. Beyond this point, recovery declined, reaching 9.53 g/100 g at CHF 32.28. As discussed previously, increasing CHF, reflecting harsher pretreatment conditions, initially led to a higher total sugar yield, which peaked and then declined due to sugar degradation. Enzymatic hydrolysis contributed an additional portion to the total recovered sugar. This trend closely followed the pattern of sugar yield from $FeCl_3$-HTP alone, which contributed up to 64 % of the total recovered sugar. The highest overall recovery was achieved at CHF 5.58, corresponding to 150 °C and 60 mM $FeCl_3$. Notably, this performance far exceeded that of non-catalyzed HTP at 150 °C, which yielded only 4.13 g/100 g CCH. In contrast, $FeCl_3$-HTP achieved up to 5.34 times higher sugar recovery, demonstrating the significant catalytic enhancement provided by $FeCl_3$ during both pretreatment and subsequent enzymatic hydrolysis. Furthermore, the successful use of CHF to describe the

Table 3
Energy consumption comparison among pretreatments

Pretreatment	Biomass	E_{eff} (kg FS/kWh)	References
HTP only (150 °C, 30 min)	CCH	0.003	This study
$FeCl_3$-HTP (150 °C, 60 mM, 30 min)	CCH	0.034	This study
Dilute acid-HTP (140 °C, 1 % (*v*/*v*) H_2SO_4, 20 min)	Grass silage	0.063	(Lin et al., 2020)
Alkaline-microwave pretreatment (300 W, 10 min, 1 % (*w*/*v*)	Sweet sorghum bagasse	0.051	(Vintila et al., 2019)
Microwave pretreatment (300 W, 10 min)	Urban green waste	0.072 (any solubilized sugar)	(Li et al., 2025)

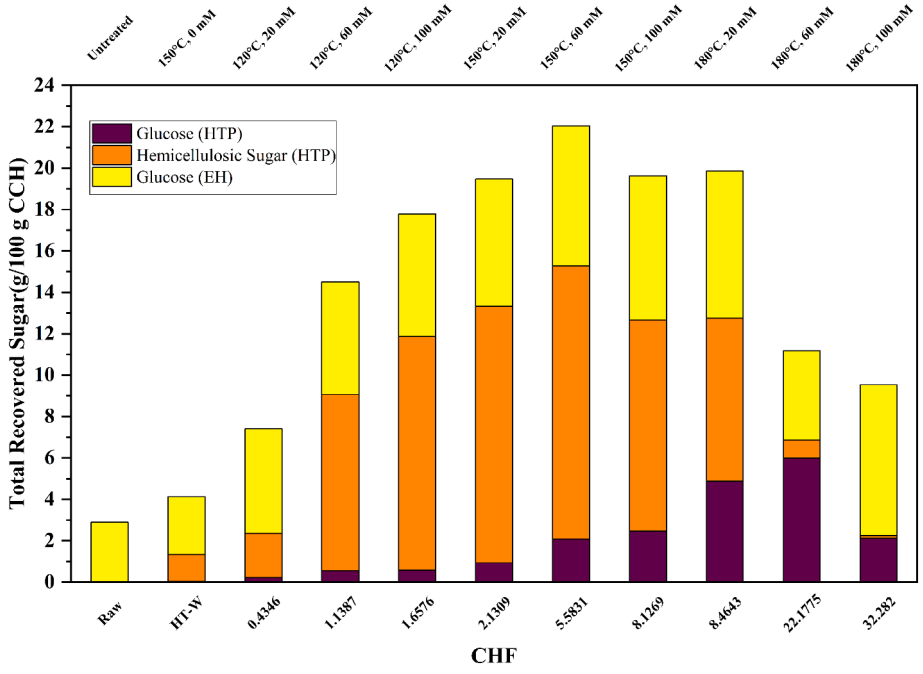

Fig. 7. Total recovered sugar from HTP coupled with EH (enzymatic hydrolysis)

pretreatment performance and its impact on total sugar recovery reinforces the robustness of this parameter and its applicability for scale-up (Jiang et al., 2023; Ruiz et al., 2021).

From an energy standpoint, the $FeCl_3$-catalyzed hydrothermal pretreatment (HTP) of CCH demonstrates a marked improvement in fermentable sugar (FS) yield per kWh, energy efficiency (E_{eff}), increasing from 0.003 kg FS/kWh with HTP alone to 0.034 kg FS/kWh with $FeCl_3$ addition (Table S4), representing an approximately tenfold enhancement. This gain follows rising CHF values and stems from increased FS production. However, under severe conditions (temperature > 150 °C or $FeCl_3$ > 60 mM), E_{eff} declines as sugar yield falls and energy input rises. When compared with other pretreatment systems (Table 3), $FeCl_3$-HTP remains competitive, hydrothermal pretreatment of grass silage, has been analyzed with competing sugar production and energy consumption, yield comparable E_{eff} targets (Lin et al., 2020). Microwave-assisted pretreatments also reduce energy consumption through direct internal heating and shorter reaction times, though most studies primarily highlight enhanced saccharification efficiency rather than explicit energy metrics (Li et al., 2025; Vintila et al., 2019). Conventional dilute acid pretreatment with sulfuric acid achieves comparable FS yields but suffers from high corrosivity and irreversible catalyst use. In contrast, Lewis acid catalysis using $FeCl_3$ is less corrosive and allows for catalyst recovery, providing potential cost advantages (Y. Zhang et al., 2023b). While microwave-assisted approaches offer efficiency and short time of process, their higher capital costs may impede industrial scalability (Siddique et al., 2022). Overall, $FeCl_3$-HTP offers a balanced profile, combining favorable energy efficiency, reduced corrosivity, and catalyst reuse potential (Moodley et al., 2020). Future work should investigate the trade-offs between maximizing E_{eff}, integrating $FeCl_3$ recovery, and optimizing downstream detoxification to enhance both technical and economic viability.

From the mass balance aspect, the best result from the mass balance calculation is presented in Fig. 8. Starting with 100 g of raw CCH, which initially contained 24.7 g hemicellulose, 38.3 g cellulose, and 36.9 g lignin, the $FeCl_3$-HTP process separated the biomass into two fractions: a solid residue and a solubilized liquid fraction. The pretreatment produced 71.5 g of solid residue, enriched in cellulose (32.4 g) and lignin (34.6 g), while the hemicellulose content significantly decreased to 4.9 g, indicating substantial hemicellulose removal. Meanwhile, the liquid fraction contained 28.5 g of solubilized CCH, including 2.1 g glucose and 13.2 g hemicellulosic sugars, meanwhile containing some degradation products, 1.9 g furfural, 1.5 g acetic acid, 0.7 g 5-HMF and 0.7 g formic acid, confirming the selective solubilization of hemicellulose during pretreatment. Subsequently, the solid residue was then subjected to enzymatic hydrolysis, releasing an additional 6.8 g of glucose, primarily targeting the cellulose preserved after pretreatment.

Table 4
Previous hydrothermal fractionation study of CCH and other biomass.

Process	Conditions	Total recovered sugar (per 100 g raw biomass)	References
HTP of CCH	259 °C, 30 min	3.39	(Prado et al., 2014)
SDS assisted-HTP of CCH	170 °C, 1 h, 3 % SDS	12.3	(Muharja et al., 2019)
HT-DES pretreatment coupled EH of CCH	HT: 210.7 °C, 77.9 min DES: 120 °C, 6 h	16.4	(Wijaya et al., 2025)
$FeCl_3$-HTP coupled EH of WSPR	150 °C, 20 mM $FeCl_3$, 40 min	32.33	(Lu et al., 2025)
$FeCl_3$-HTP coupled EH of CCH	150 °C, 60 mM $FeCl_3$, 30 min	22.04	This study

HT: hydrothermal; HTP: HTP; DES: deep eutectic solvent; EH: enzymatic hydrolysis; SDS: sodium dodecyl sulphate; WSPR: wheat straw pulp residue

The high lignin content remaining in the solid fraction following $FeCl_3$-HTP offers a promising opportunity for further valorization, particularly through lignin recovery and utilization strategies, which may enhance the overall economic feasibility of integrating pretreatment and biorefinery processes for CCH (Fernández Méndez et al., 2023; Yiin et al., 2024). Previous studies have reported that metal salt-assisted hydrothermal pretreatment can alter the structural characteristics of lignin. For example, significant cleavage of β-O-4 ether linkages was observed, while syringyl (S) and guaiacyl (G) units largely remained intact, suggesting selective lignin depolymerization without extensive aromatic unit degradation (Shen et al., 2016). This structural transformation is advantageous, as it may facilitate lignin solubilization in subsequent pretreatment steps, such as deep eutectic solvents (DES), when employed in a sequential or synergistic configuration. Furthermore, the isolated lignin, due to its preserved structural motifs, holds potential for conversion into functional materials or platform chemicals. Simultaneously, such pretreatment strategies contribute to improved enzymatic saccharification by reducing biomass recalcitrance (Shen et al., 2021; Wijaya et al., 2025).

Findings from previous studies on CCH and other biomass fractionation for sugar recovery are summarized in Table 4. HTP alone has been reported to produce only 3.39 g sugar per 100 g raw CCH, even at a high temperature of 259 °C (Prado et al., 2014). Efforts to enhance sugar recovery by incorporating the surfactant SDS has reported in a higher yield of 12.3 g sugar per 100 g raw CCH. The addition of surfactant

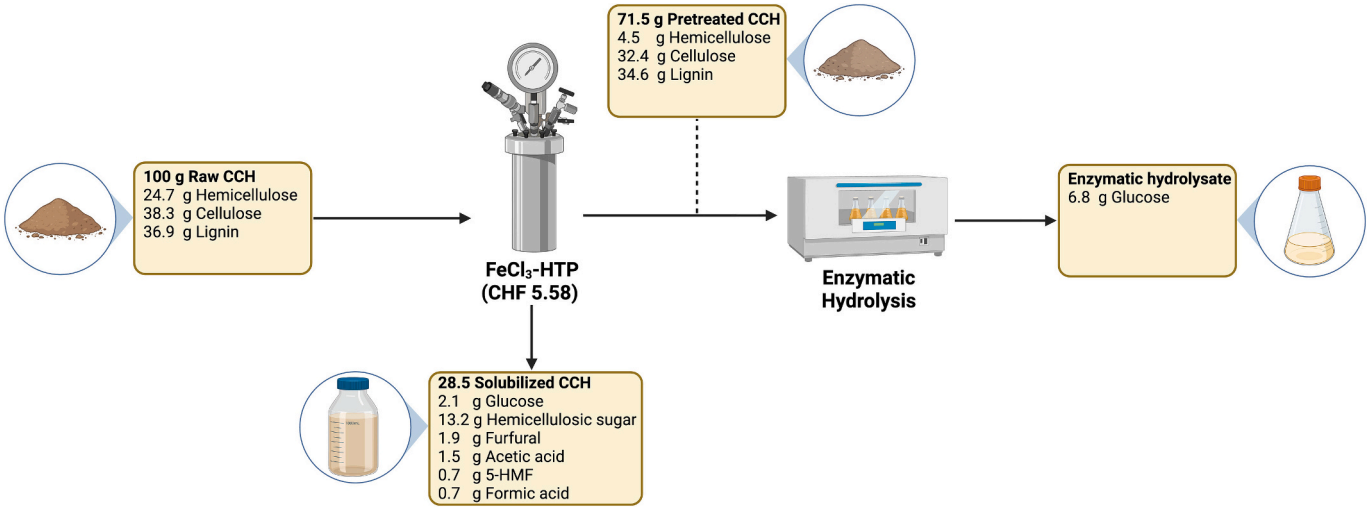

Fig. 8. Process mass balance of highest total recovered sugar in $FeCl_3$-HTP with basis 100 g raw CCH

facilitated enhanced solubilization of sugars and lignin, contributing to improved sugar release during HTP [65]. Sequential pretreatment involving HTP followed by deep eutectic solvent (DES) ptreatment has also been reported to further increase sugar recovery, reaching 16.4 g per 100 g raw CCH. This multi-step strategy offers a selective approach for fractionating hemicellulosic sugars and lignin, thereby enhancing enzymatic hydrolysis yields while preserving other fractions such as lignin (Wijaya et al., 2025). In comparison, $FeCl_3$-HTP coupled with EH of WSPR achieved 32.23 g of sugar per 100 g WSPR, demonstrating high monomeric sugar yield with a similar process to this study (Lu et al., 2025). The lower lignin content in WSPR likely contributed to the higher sugar yield compared to CCH.

Notably, the present study demonstrates that even with a single-step pretreatment, $FeCl_3$-catalyzed HTP coupled with enzymatic hydrolysis can achieve higher sugar recovery than these previous approaches. This highlights the effectiveness of $FeCl_3$ as a metal salt catalyst in enhancing sugar release since only one pretreatment needed. The findings support the potential of CCH valorization into economically valuable products, such as biofuels or biochemicals, advancing the integration of CCH into biorefinery frameworks.

4. Conclusions

This study demonstrated the effectiveness of $FeCl_3$-HTP in enhancing sugar yield compared to conventional hydrothermal methods. Using CCH as a representative lignocellulosic biomass, $FeCl_3$-HTP significantly improved hemicellulose solubilization, hemicellulosic sugar and glucose yields, and enzymatic digestibility. The CHF was successfully applied as a unifying severity parameter, providing a strong predictive tool for correlating xylan conversion with pretreatment conditions. Mass balance analysis indicated that moderate CHF values (around 5.58) yielded the highest total sugar recovery (22.04 g/100 g CCH), representing a 5.34-fold improvement over non-catalyzed pretreatment at the same temperature. Structural and compositional changes, confirmed by XRD, SEM, and FTIR, supported the role of $FeCl_3$ in selectively disrupting hemicellulose and enhancing enzyme accessibility without causing excessive cellulose degradation. Future work should focus on refining kinetic models based on CHF for hemicellulosic sugar prediction and exploring the valorization of the residual lignin fraction to support the sustainability and economic feasibility of large-scale CCH fractionation. Moreover, the promising results observed in this study suggest that the method could be effectively extended to other lignocellulosic feedstocks, such as oil palm empty fruit bunches and rice straw, for high-value bioproduct generation.

CRediT authorship contribution statement

Candra Wijaya: Writing – original draft, Visualization, Software, Methodology, Investigation, Formal analysis, Conceptualization. **Ningsi Lick Sangadji:** Writing – review & editing. **Maktum Muharja:** Writing – review & editing. **Tri Widjaja:** Writing – review & editing, Supervision. **Lieke Riadi:** Writing – review & editing, Supervision. **Elaine Elaine:** Writing – review & editing. **Raymond Lau:** Writing – review & editing, Validation, Supervision. **Arief Widjaja:** Writing – review & editing, Supervision, Project administration, Data curation, Conceptualization.

Declaration of competing interest

The authors declare that they have no known competing financial interests or personal relationships that could have appeared to influence the work reported in this paper.

Acknowledgment

The authors are grateful for the research support provided by the Indonesia Endowment Fund for Education (LPDP) on behalf of the Indonesia Ministry of Education, Culture, Research and Technology and managed by Institut Teknologi Sepuluh Nopember under INSPIRASI Program (Grant No PRJ-61/LPDP/2022 and 2965/E3/AL.04/2024).

Appendix A. Supplementary data

Supplementary data to this article can be found online at https://doi.org/10.1016/j.biteb.2025.102282.

Data availability

Data will be made available on request.

References

Abouelela, A.R., Nakasu, P.Y.S., Hallett, J.P., 2023. Influence of pretreatment severity factor and hammett acidity on softwood fractionation by an acidic protic ionic liquid. ACS Sustain. Chem. Eng. 11, 2404–2415. https://doi.org/10.1021/acssuschemeng.2c06076.

Aline Otaviano, C., Ussemane Mussagy, C., Roberto Paz-Cedeno, F., Fernando Brandão Pereira, J., Masarin, F., 2023. Hydrothermal pretreatment of Eucalyptus by-product and refining of xylooligosaccharides from hemicellulosic hydrolysate. Sep. Purif. Technol. 306. https://doi.org/10.1016/j.seppur.2022.122520.

Anuchi, S.O., Campbell, K.L.S., Hallett, J.P., 2022. Effective pretreatment of lignin-rich coconut wastes using a low-cost ionic liquid. Sci. Rep. 12, 1–11. https://doi.org/10.1038/s41598-022-09629-4, 2022 12:1.

Basak, B., Kumar, R., Bharadwaj, A.V.S.L.S., Kim, T.H., Kim, J.R., Jang, M., Oh, S.E., Roh, H.S., Jeon, B.H., 2023. Advances in physicochemical pretreatment strategies for lignocellulose biomass and their effectiveness in bioconversion for biofuel production. Bioresour. Technol. 369. https://doi.org/10.1016/j.biortech.2022.128413.

Bhatia, S.K., Jagtap, S.S., Bedekar, A.A., Bhatia, R.K., Patel, A.K., Pant, D., Rajesh Banu, J., Rao, C.V., Kim, Y.G., Yang, Y.H., 2020. Recent developments in pretreatment technologies on lignocellulosic biomass: effect of key parameters, technological improvements, and challenges. Bioresour. Technol. 300, 122724. https://doi.org/10.1016/j.biortech.2019.122724.

Chen, Y.W., Lee, H.V., 2020. Recent progress in homogeneous Lewis acid catalysts for the transformation of hemicellulose and cellulose into valuable chemicals, fuels, and nanocellulose. Rev. Chem. Eng. 36, 215–235. https://doi.org/10.1515/revce-2017-0071.

Chen, L., Chen, R., Fu, S., 2014. Preliminary exploration on pretreatment with metal chlorides and enzymatic hydrolysis of bagasse. Biomass Bioenergy 71, 311–317. https://doi.org/10.1016/j.biombioe.2014.09.026.

Chen, L., Chen, R., Fu, S., 2015. FeCl3 pretreatment of three lignocellulosic biomass for ethanol production. ACS Sustain. Chem. Eng. 3, 1794–1800. https://doi.org/10.1021/acssuschemeng.5b00377.

Chen, W.-H., Nižetić, S., Sirohi, R., Huang, Z., Luque, R., M. Papadopoulos, A., Sakthivel, R., Phuong Nguyen, X., Tuan Hoang, A., 2022. Liquid hot water as sustainable biomass pretreatment technique for bioenergy production: a review. Bioresour. Technol. 344, 126207. https://doi.org/10.1016/j.biortech.2021.126207.

Clauser, N.M., Fit, C.G., Cardozo, R.E., Rivaldi, J.A., Felissia, F.E., Area, M.C., Vallejos, M.E., 2024. Technical, economic and environmental assessment of xylitol production in a biorefinery platform toward a circular economy. Sustainability 16, 1–21. https://doi.org/10.3390/su162310770 Academic.

Curry, T.M., Peña, M.J., Urbanowicz, B.R., 2023. An update on xylan structure, biosynthesis, and potential commercial applications. Cell Surf. https://doi.org/10.1016/j.tcsw.2023.100101.

du Pasquier, J., Paës, G., Perré, P., 2024. Chemical degradation, yields, and interactions of lignocellulosic compounds of poplar wood during dilute acid pretreatment assessed from a comprehensive data set. Ind. Crops Prod. 215. https://doi.org/10.1016/j.indcrop.2024.118643.

Esmaeilbeig, M.A., Khorram, M., Ayatollahi, S., Zolghadr, A.R., 2022. On the hydrolysis of iron ions: DFT-based molecular dynamics perspective. J. Mol. Liq. 367. https://doi.org/10.1016/j.molliq.2022.120323.

Felipe Hernández-Pérez, A., de Arruda, P.V., Sene, L., da Silva, S.S., Kumar Chandel, A., de Almeida Felipe, M. das G., 2019. Xylitol bioproduction: state-of-the-art, industrial paradigm shift, and opportunities for integrated biorefineries. Crit. Rev. Biotechnol. 39, 924–943. https://doi.org/10.1080/07388551.2019.1640658.

Fernández Méndez, J., Farfan Orozco, F., Ladero Galán, M., Grénman, H., 2023. Techno-economic evaluation of obtaining valuable rare sugars from thermo-mechanical pulping side streams utilizing the latest technology. Chem. Eng. J. 455, 140852. https://doi.org/10.1016/J.CEJ.2022.140852.

Gao, K., Chen, Y., Wang, H., Quan, X., Chu, J., Zhang, J., 2023. Production of xylooligosaccharides and monosaccharides from switchgrass by FeCl3 hydrolysis combined with sodium perborate pretreatment. Bioenergy Res. 16, 2242–2252. https://doi.org/10.1007/s12155-023-10573-y.

Gao, Q., Tang, Z., He, Y.C., 2025. Valorization of wheat straw through enhancement of cellulose accessibility, xylan elimination and lignin removal by choline chloride:p-toluenesulfonic acid pretreatment. Int. J. Biol. Macromol. 301. https://doi.org/10.1016/j.ijbiomac.2025.140335.

Geng, W., Narron, R., Jiang, X., Pawlak, J.J., Chang, H. min, Park, S., Jameel, H., Venditti, R.A., 2019. The influence of lignin content and structure on hemicellulose alkaline extraction for non-wood and hardwood lignocellulosic biomass. Cellulose 26, 3219–3230. https://doi.org/10.1007/s10570-019-02261-y.

Giummarella, N., Lawoko, M., 2017. Structural insights on recalcitrance during hydrothermal hemicellulose extraction from wood. ACS Sustain. Chem. Eng. 5, 5156–5165. https://doi.org/10.1021/acssuschemeng.7b00511.

Gundupalli, M.P., Tantayotai, P., Panakkal, E.J., Chuetor, S., Kirdponpattara, S., Thomas, A.S.S., Sharma, B.K., Sriariyanun, M., 2022. Hydrothermal pretreatment optimization and deep eutectic solvent pretreatment of lignocellulosic biomass: an integrated approach. Bioresour. Technol. Rep. 100957. https://doi.org/10.1016/j.biteb.2022.100957.

Hames, B., Ruiz, R., Scarlata, C., Sluiter, A., Sluiter, J., Templeton, D., 2008. Preparation of Samples for Compositional Analysis: Laboratory Analytical Procedure (LAP); Issue Date 08/08/2008.

Huang, K., Das, L., Guo, J., Xu, Y., 2019. Catalytic valorization of hardwood for enhanced xylose-hydrolysate recovery and cellulose enzymatic efficiency via synergistic effect of Fe3+ and acetic acid. Biotechnol. Biofuels 12. https://doi.org/10.1186/s13068-019-1587-4.

Huo, D., Sun, Y., Yang, Q., Zhang, F., Fang, G., Zhu, H., Liu, Y., 2023. Selective degradation of hemicellulose and lignin for improving enzymolysis efficiency via pretreatment using deep eutectic solvents. Bioresour. Technol. 376, 128937. https://doi.org/10.1016/j.biortech.2023.128937.

Ilanidis, D., Stagge, S., Jönsson, L.J., Martín, C., 2021. Effects of operational conditions on auto-catalyzed and sulfuric-acid-catalyzed hydrothermal pretreatment of sugarcane bagasse at different severity factor. Ind. Crops Prod. 159. https://doi.org/10.1016/j.indcrop.2020.113077.

Ji, H., Song, Y., Zhang, X., Tan, T., 2017. Using a combined hydrolysis factor to balance enzymatic saccharification and the structural characteristics of lignin during pretreatment of Hybrid poplar with a fully recyclable solid acid. Bioresour. Technol. 238, 575–581. https://doi.org/10.1016/j.biortech.2017.04.092.

Jia, Y., Yang, C., Shen, B., Ling, Z., Huang, C., Li, X., Lai, C., Yong, Q., 2021. Comparative study on enzymatic digestibility of acid-pretreated poplar and larch based on a comprehensive analysis of the lignin-derived recalcitrance. Bioresour. Technol. 319. https://doi.org/10.1016/j.biortech.2020.124225.

Jiang, X., Zhai, R., Li, H., Li, C., Deng, Q., Jin, M., 2023. Understanding acid hydrolysis of corn stover during densification pretreatment for quantitative predictions of enzymatic hydrolysis efficiency using modified pretreatment severity factor. Bioresour. Technol. 386. https://doi.org/10.1016/j.biortech.2023.129487.

Kamireddy, S.R., Li, J., Tucker, M., Degenstein, J., Ji, Y., 2013. Effects and mechanism of metal chloride salts on pretreatment and enzymatic digestibility of corn stover. Ind. Eng. Chem. Res. 52, 1775–1782. https://doi.org/10.1021/ie3019609.

Kaur, G., Kaur, P., Kaur, J., Singla, D., Taggar, M.S., 2024. Xylanase, xylooligosaccharide and xylitol production from lignocellulosic biomass: exploring biovalorization of xylan from a sustainable biorefinery perspective. Ind. Crop. Prod. https://doi.org/10.1016/j.indcrop.2024.118610.

Kininge, M.M., Gogate, P.R., 2022. Intensification of alkaline delignification of sugarcane bagasse using ultrasound assisted approach. Ultrason. Sonochem. 82. https://doi.org/10.1016/J.ULTSONCH.2021.105870.

Kumar, R., Mago, G., Balan, V., Wyman, C.E., 2009. Physical and chemical characterizations of corn stover and poplar solids resulting from leading pretreatment technologies. Bioresour. Technol. 100, 3948–3962. https://doi.org/10.1016/j.biortech.2009.01.075.

Kumar, B., Bhardwaj, N., Verma, P., 2019. Pretreatment of rice straw using microwave assisted FeCl3-H3PO4 system for ethanol and oligosaccharides generation. Bioresour. Technol. Rep. 7. https://doi.org/10.1016/j.biteb.2019.100295.

Labauze, H., Benjelloun-Mlayah, B., 2021. Kinetics of xylan hydrolysis using an acetic and formic acid-based organosolv pretreatment. Bioresour. Technol. Rep. 14, 100690. https://doi.org/10.1016/j.biteb.2021.100690.

Leal Silva, J.F., Nakasu, P.Y.S., Costa, A.C. da, Maciel Filho, R., Rabelo, S.C., 2022. Techno-economic analysis of the production of 2G ethanol and technical lignin via a protic ionic liquid pretreatment of sugarcane bagasse. Ind. Crops Prod. 189. https://doi.org/10.1016/j.indcrop.2022.115788.

Li, M., Cao, S., Meng, X., Studer, M., Wyman, C.E., Ragauskas, A.J., Pu, Y., 2017. The effect of liquid hot water pretreatment on the chemical-structural alteration and the reduced recalcitrance in poplar. Biotechnol. Biofuels 10. https://doi.org/10.1186/s13068-017-0926-6.

Li, W.X., Xiao, W.Z., Yang, Y.Q., Wang, Q., Chen, X., Xiao, L.P., Sun, R.C., 2021. Insights into bamboo delignification with acidic deep eutectic solvents pretreatment for enhanced lignin fractionation and valorization. Ind. Crops Prod. 170. https://doi.org/10.1016/j.indcrop.2021.113692.

Li, Jianzheng, Liu, W., Meng, J., Zhao, L., Li, Jiuling, Zheng, M., 2022. Mesothermal pretreatment using FeCl3 enhances methane production from rice straw. Renew. Energy 188, 670–677. https://doi.org/10.1016/j.renene.2022.02.028.

Li, J., Tan, J., Zhang, B., Wei, C., Li, P., Zhang, Y., Chen, J., 2025. Microwave assisted pretreatment of urban green waste with more efficiency and less energy cost. Int. J. Environ. Sci. Technol. 22, 1107–1122. https://doi.org/10.1007/s13762-024-05736-z.

Lin, R., Deng, C., Rajendran, K., Bose, A., Kang, X., Murphy, J.D., 2020. Competing reactions limit production of sugars in hydrothermal hydrolysis of grass silage: an assessment of the effect of temperature on sugar production and parasitic energy demand. Front. Energy Res. 8. https://doi.org/10.3389/fenrg.2020.575523.

Liu, H., Zhang, J., Yuan, J., Jiang, X., Jiang, L., Zhao, G., Huang, D., Liu, B., 2019. Omics-based analyses revealed metabolic responses of Clostridium acetobutylicum to lignocellulose-derived inhibitors furfural, formic acid and phenol stress for butanol fermentation. Biotechnol. Biofuels 12. https://doi.org/10.1186/s13068-019-1440-9.

Liu, C., Choi, B., Efimova, E., Nygård, Y., Santala, S., 2024a. Enhanced upgrading of lignocellulosic substrates by coculture of Saccharomyces cerevisiae and Acinetobacter baylyi ADP1. Biotechnol. Biofuels Bioprod. 17. https://doi.org/10.1186/s13068-024-02510-8.

Liu, Y., Ding, Y., Li, Y., Wang, X., Sun, Y., Chen, C., 2024b. A comprehensive review of recent advances in delignification technology. J. Text. Inst. 115, 2489–2504. https://doi.org/10.1080/00405000.2023.2296691.

López-Linares, J.C., Romero, I., Moya, M., Cara, C., Ruiz, E., Castro, E., 2013. Pretreatment of olive tree biomass with FeCl3 prior enzymatic hydrolysis. Bioresour. Technol. 128, 180–187. https://doi.org/10.1016/j.biortech.2012.10.076.

Lu, K., Fan, Z., Liao, Y., Wu, X., Liu, H., Jin, M., Wang, H., Han, S., Zhang, Y., Sun, F., 2025. Enhancing the enzymatic hydrolysis efficiency of wheat straw pulp residue by prewashing and ferric chloride assisted hydrothermal pretreatment. Ind. Crops Prod. 223. https://doi.org/10.1016/j.indcrop.2024.120238.

Lv, Y., Zhang, Y., Xu, Y., 2024. Understanding and technological approach of acid hydrolysis processing for lignocellulose biorefinery: panorama and perspectives. Biomass Bioenergy. https://doi.org/10.1016/j.biombioe.2024.107133.

Ma, Q., Zhu, J., Gleisner, R., Yang, R., Zhu, J.Y., 2018. Valorization of wheat straw using a recyclable hydrotrope at low temperatures (≤90 °c). ACS Sustain. Chem. Eng. 6, 14480–14489. https://doi.org/10.1021/acssuschemeng.8b03135.

Ma, C.Y., Xu, L.H., Zhang, C., Guo, K.N., Yuan, T.Q., Wen, J.L., 2021. A synergistic hydrothermal-deep eutectic solvent (DES) pretreatment for rapid fractionation and targeted valorization of hemicelluloses and cellulose from poplar wood. Bioresour. Technol. 341, 125828. https://doi.org/10.1016/j.biortech.2021.125828.

Mankar, A.R., Pandey, A., Pant, K.K., 2022. Microwave-assisted extraction of lignin from coconut coir using deep eutectic solvents and its valorization to aromatics. Bioresour. Technol. 345. https://doi.org/10.1016/j.biortech.2021.126528.

Marecka-Migacz, A., Mitkowski, P.T., Nędzarek, A., Różański, J., Szaferski, W., 2020. Effect of pH on total volume membrane charge density in the nanofiltration of aqueous solutions of nitrate salts of heavy metals. Membranes (Basel) 10, 235. https://doi.org/10.3390/membranes10090235.

Millán Acosta, A., Cosovanu, D., Cabañeros López, P., Thomsen, S.T., Gernaey, K.V., Canela-Garayoa, R., 2021. Co-cultivation of a novel Fusarium striatum strain and a xylose consuming Saccharomyces cerevisiae yields an efficient process for simultaneous detoxification and fermentation of lignocellulosic hydrolysates. Chem. Eng. J. 426. https://doi.org/10.1016/j.cej.2021.131575.

Mittal, A., Vinzant, T.B., Brunecky, R., Black, S.K., Pilath, H.M., Himmel, M.E., Johnson, D.K., 2015. Investigation of the role of lignin in biphasic xylan hydrolysis during dilute acid and organosolv pretreatment of corn stover. Green Chem. 17, 1546–1558. https://doi.org/10.1039/c4gc02258k.

Moodley, P., Sewsynker-Sukai, Y., Gueguim Kana, E.B., 2020. Progress in the development of alkali and metal salt catalysed lignocellulosic pretreatment regimes: potential for bioethanol production. Bioresour. Technol. https://doi.org/10.1016/j.biortech.2020.123372.

Mu, X., Han, Z., Liu, C., Zhang, D., 2019. Mechanistic insights into formaldehyde-blocked lignin condensation: a DFT study. J. Phys. Chem. C 123, 8640–8648. https://doi.org/10.1021/acs.jpcc.9b00247.

Muharja, M., Junianti, F., Ranggina, D., Nurtono, T., Widjaja, A., 2018. An integrated green process: subcritical water, enzymatic hydrolysis, and fermentation, for biohydrogen production from coconut husk. Bioresour. Technol. 249, 268–275. https://doi.org/10.1016/j.biortech.2017.10.024.

Muharja, M., Umam, D.K., Pertiwi, D., Zuhdan, J., Nurtono, T., Widjaja, A., 2019. Enhancement of sugar production from coconut husk based on the impact of the combination of surfactant-assisted subcritical water and enzymatic hydrolysis. Bioresour. Technol. 274, 89–96. https://doi.org/10.1016/j.biortech.2018.11.074.

Prado, J.M., Forster-Carneiro, T., Rostagno, M.A., Follegatti-Romero, L.A., Maugeri Filho, F., Meireles, M.A.A., 2014. Obtaining sugars from coconut husk, defatted grape seed, and pressed palm fiber by hydrolysis with subcritical water. J. Supercrit. Fluids 89, 89–98. https://doi.org/10.1016/j.supflu.2014.02.017.

Rathour, R.K., Behl, M., Dhashmana, K., Sakhuja, D., Ghai, H., Sharma, N., Meena, K.R., Bhatt, A.K., Bhatia, R.K., 2023. Non-food crops derived lignocellulose biorefinery for sustainable production of biomaterials, biochemicals and bioenergy: a review on trends and techniques. Ind. Crops Prod. 204, 117220. https://doi.org/10.1016/j.indcrop.2023.117220.

Rodríguez-Rebelo, F., Rodríguez-Martínez, B., Del-Río, P.G., Collins, M.N., Garrote, G., Gullón, B., 2024. Assessment of deep eutectic solvents (DES) to fractionate Paulownia wood within a biorefinery scheme: Cellulosic bioethanol production and lignin isolation. Ind. Crops Prod. 216. https://doi.org/10.1016/j.indcrop.2024.118761.

Romero, I., López-Linares, J.C., Moya, M., Castro, E., 2018. Optimization of sugar recovery from rapeseed straw pretreated with FeCl3. Bioresour. Technol. 268, 204–211. https://doi.org/10.1016/j.biortech.2018.07.112.

Ruiz, H.A., Conrad, M., Sun, S.N., Sanchez, A., Rocha, G.J.M., Romaní, A., Castro, E., Torres, A., Rodríguez-Jasso, R.M., Andrade, L.P., Smirnova, I., Sun, R.C., Meyer, A. S., 2020. Engineering aspects of hydrothermal pretreatment: from batch to continuous operation, scale-up and pilot reactor under biorefinery concept. Bioresour. Technol. 299, 122685. https://doi.org/10.1016/j.biortech.2019.122685.

Ruiz, H.A., Galbe, M., Garrote, G., Ramirez-Gutierrez, D.M., Ximenes, E., Sun, S.N., Lachos-Perez, D., Rodríguez-Jasso, R.M., Sun, R.C., Yang, B., Ladisch, M.R., 2021. Severity factor kinetic model as a strategic parameter of hydrothermal processing (steam explosion and liquid hot water) for biomass fractionation under biorefinery concept. Bioresour. Technol. 342, 125961.

Ruiz, H.A., Sganzerla, W.G., Larnaudie, V., Veersma, R.J., van Erven, G., Shiva L.J., Ríos-González, Rodríguez-Jasso, R.M., Rosero-Chasoy, G., Ferrari, M.D., Kabel, M.A., Forster-Carneiro, T., Lareo, C., 2023. Advances in process design, techno-economic assessment and environmental aspects for hydrothermal pretreatment in the

fractionation of biomass under biorefinery concept. Bioresour. Technol. https://doi.org/10.1016/j.biortech.2022.128469.
Saini, R., Singhania, R.R., Patel, A.K., Chen, C.W., Piechota, G., Di Dong, C., 2024. Sustainable production of cellulose and hemicellulose-derived oligosaccharides from pineapple leaves: Impact of hydrothermal pretreatment and controlled enzymatic hydrolysis. Bioresour. Technol. 398, 130526. https://doi.org/10.1016/J.BIORTECH.2024.130526.
Sangadji, N.L., Wijaya, C., Sangian, H.F., Widjaja, A., 2024. Optimization of ultrasound-enhanced subcritical water hydrolysis of oil palm empty fruit bunch for the production of fermentable sugar. Period. Polytech. Chem. Eng. 68, 203–215. https://doi.org/10.3311/PPch.23183.
Shah, A.M., Kamal, R., Wang, Q., Zhang, J., Lu, H., Zhao, Z.K., 2025. Calcium carbonate-mediated detoxification of corn stover hydrolysate to facilitate the fermentation by Rhodosporidium toruloides. Biomass Bioenergy 200. https://doi.org/10.1016/j.biombioe.2025.108036.
Shen, X.J., Wang, B., Huang, P.L., Wen, J.L., Sun, R.C., 2016. Effects of aluminum chloride-catalyzed hydrothermal pretreatment on the structural characteristics of lignin and enzymatic hydrolysis. Bioresour. Technol. 206, 57–64. https://doi.org/10.1016/j.biortech.2016.01.031.
Shen, B., Hou, S., Jia, Y., Yang, C., Su, Y., Ling, Z., Huang, C., Lai, C., Yong, Q., 2021. Synergistic effects of hydrothermal and deep eutectic solvent pretreatment on co-production of xylo-oligosaccharides and enzymatic hydrolysis of poplar. Bioresour. Technol. 341, 125787. https://doi.org/10.1016/j.biortech.2021.125787.
Shi, R., Zhang, Z., Zhang, J., Chen, C., Li, W., Lin, Y., Shi, X., Zhao, P., Zhang, T., Yan, Q., Cheng, X., 2025. A comparative study on enhanced enzymatic hydrolysis of diverse herbaceous and woody wastes by promising dilute acid and alkaline pretreatments. Bioresour. Bioprocess. 12. https://doi.org/10.1186/s40643-025-00873-w.
Siddique, I.J., Salema, A.A., Antunes, E., Vinu, R., 2022. Technical challenges in scaling up the microwave technology for biomass processing. Renew. Sustain. Energy Rev. 153, 111767. https://doi.org/10.1016/J.RSER.2021.111767.
Sluiter, A., 2008. Determination of Structural Carbohydrates and Lignin in Biomass. Laboratory Analytical Procedure (LAP)/National Renewable Energy Laboratory.
Springer, E.L., 1966. Hydrolysis of aspenwood xylan with aqueous solutions of hydrochloric acid. Tappi 49, 102.
Su, Y., Wang, P., Lai, C., Huang, C., Ling, Z., Yong, Q., 2023. Revealing key factors influencing enzymatic digestibility of hydrothermally pretreated poplar in comparison with corn stover. Ind. Crop. Prod. 194. https://doi.org/10.1016/j.indcrop.2023.116297.
Sun, Q., Chen, W.J., Pang, B., Sun, Z., Lam, S.S., Sonne, C., Yuan, T.Q., 2021. Ultrastructural change in lignocellulosic biomass during hydrothermal pretreatment. Bioresour. Technol. 341, 125807. https://doi.org/10.1016/j.biortech.2021.125807.
Tan, L., Liu, Z., Zhang, T., Wang, Z., Liu, T., 2020. Enhanced enzymatic digestibility of poplar wood by quick hydrothermal treatment. Bioresour. Technol. 302. https://doi.org/10.1016/j.biortech.2020.122795.
Tang, W., Wu, X., Huang, C., Ling, Z., Lai, C., Yong, Q., 2021. Revealing the influence of metallic chlorides pretreatment on chemical structures of lignin and enzymatic hydrolysis of waste wheat straw. Bioresour. Technol. 342, 125983. https://doi.org/10.1016/J.BIORTECH.2021.125983.
Tang, W., Huang, C., Ling, Z., Lai, C., Yong, Q., 2022. Efficient utilization of waste wheat straw through humic acid and ferric chloride co-assisted hydrothermal pretreatment for fermentation to produce bioethanol. Bioresour. Technol. 364. https://doi.org/10.1016/j.biortech.2022.128059.
Tang, Z., Wu, C., Tang, W., Huang, M., Ma, C., He, Y.-C., 2023. Enhancing enzymatic saccharification of sunflower straw through optimal tartaric acid hydrothermal pretreatment. Bioresour. Technol. 385, 129279. https://doi.org/10.1016/j.biortech.2023.129279.
Vieira, F., Santana, E.P., Jesus, M., Santos, J., Pires, P., Vaz-velho, M., Silva, D.P., Ruzene, D.S., 2024. Coconut waste: discovering sustainable approaches to advance a circular economy. Sustainability 16, 1–25. https://doi.org/10.3390/su16073066 Academic.
Vintila, T., Sumalan, R., Popa, N.F., Dragomirescu, M., Sala, F., 2019. Microwave and steam mediated alkaline pretreatments of sweet sorghum bagasse: study of the energy efficiency. Bioresources 14, 4022–4034. https://doi.org/10.15376/biores.14.2.4022-4034.
Wan, G., Zhang, Q., Li, M., Jia, Z., Guo, C., Luo, B., Wang, S., Min, D., 2019. How pseudo-lignin is generated during dilute sulfuric acid pretreatment. J. Agric. Food Chem. 67, 10116–10125. https://doi.org/10.1021/acs.jafc.9b02851.
Wang, R., Wang, K., Zhou, M., Xu, J., Jiang, J., 2021. Efficient fractionation of moso bamboo by synergistic hydrothermal-deep eutectic solvents pretreatment. Bioresour. Technol. 328, 124873. https://doi.org/10.1016/J.BIORTECH.2021.124873.
Warren-Walker, D., Ravella, S.R., Gallagher, J., Winters, A., Charlton, A., Bryant, D.N., 2024. Optimising parameters for pilot scale steam explosion and continuous pressurised disc refining of Miscanthus and sugarcane bagasse for xylose and xylo-oligosaccharide release. Bioresour. Technol. 405, 130932. https://doi.org/10.1016/j.biortech.2024.130932.
Wei, H., Chen, X., Shekiro, J., Kuhn, E., Wang, W., Ji, Y., Kozliak, E., Himmel, M.E., Tucker, M.P., 2018. Kinetic modelling and experimental studies for the effects of fe2 + ions on xylan hydrolysis with dilute-acid pretreatment and subsequent enzymatic hydrolysis. Catalysts 8. https://doi.org/10.3390/catal8010039.
Wijaya, C., Sangadji, N.L., Muharja, M., Widjaja, T., Riadi, L., Widjaja, A., 2025. An integrated green fractionation of coconut husk: hydrothermal and deep eutectic solvent pretreatment for enhanced sugar and lignin production. Bioresour. Technol. Rep. 102078. https://doi.org/10.1016/j.biteb.2025.102078.
Wu, X., Huang, Chen, Tang, W., Huang, Caoxing, Lai, C., Yong, Q., 2018. Use of metal chlorides during waste wheat straw autohydrolysis to overcome the self-buffering effect. Bioresour. Technol. 268, 259–265. https://doi.org/10.1016/J.BIORTECH.2018.07.132.
Wu, J., Du, X., Yin, Z., Xu, Shuang, Xu, Shuying, Zhang, Y., 2019. Preparation and characterization of cellulose nanofibrils from coconut coir fibers and their reinforcements in biodegradable composite films. Carbohydr. Polym. 211, 49–56. https://doi.org/10.1016/j.carbpol.2019.01.093.
Xiao, L.P., Shi, Z.J., Bai, Y.Y., Wang, W., Zhang, X.M., Sun, R.C., 2013. Biodegradation of lignocellulose by white-rot fungi: structural characterization of water-soluble hemicelluloses. Bioenergy Res. 6, 1154–1164. https://doi.org/10.1007/s12155-013-9302-y.
Yaashikaa, P.R., Senthil Kumar, P., Varjani, S., 2022. Valorization of agro-industrial wastes for biorefinery process and circular bioeconomy: a critical review. Bioresour. Technol. 343, 126126. https://doi.org/10.1016/J.BIORTECH.2021.126126.
Yang, Q., Tang, W., Li, L., Huang, M., Ma, C., He, Y.-C., 2023. Enhancing enzymatic hydrolysis of waste sunflower straw by clean hydrothermal pretreatment. Bioresour. Technol. 383, 129236. https://doi.org/10.1016/j.biortech.2023.129236.
Yao, J., Xie, X., Shi, Q., 2021. Improving enzymatic saccharification of Chinese silvergrass by FeCl3-catalyzed γ-valerolactone/water pretreatment system. Renew. Energy 177, 853–858. https://doi.org/10.1016/j.renene.2021.06.009.
Yiin, C.L., Lai, Z.Y., Chin, B.L.F., Lock, S.S.M., Cheah, K.W., Taylor, M.J., Al-Gailani, A., Kolosz, B.W., Chan, Y.H., 2024. Green pathways for biomass transformation: a holistic evaluation of deep eutectic solvents (DESs) through life cycle and techno-economic assessment. J. Clean. Prod. 470. https://doi.org/10.1016/j.jclepro.2024.143248.
Zhang, C., Houtman, C.J., Zhu, J.Y., 2014. Using low temperature to balance enzymatic saccharification and furan formation during SPORL pretreatment of Douglas-fir. Process Biochem. 49, 466–473. https://doi.org/10.1016/j.procbio.2013.12.017.
Zhang, X., Zhang, W., Lei, F., Yang, S., Jiang, J., 2020. Coproduction of xylooligosaccharides and fermentable sugars from sugarcane bagasse by seawater hydrothermal pretreatment. Bioresour. Technol. 309. https://doi.org/10.1016/j.biortech.2020.123385.
Zhang, R., Gao, H., Wang, Yongtai, He, B., Lu, J., Zhu, W., Peng, L., Wang, Yanting, 2023a. Challenges and perspectives of green-like lignocellulose pretreatments selectable for low-cost biofuels and high-value bioproduction. Bioresour. Technol. 369, 128315. https://doi.org/10.1016/j.biortech.2022.128315.
Zhang, Y., Ding, Z., Shahadat Hossain, M., Maurya, R., Yang, Y., Singh, V., Kumar, D., Salama, E.S., Sun, X., Sindhu, R., Binod, P., Zhang, Z., Kumar Awasthi, M., 2023b. Recent advances in lignocellulosic and algal biomass pretreatment and its biorefinery approaches for biochemicals and bioenergy conversion. Bioresour. Technol. 367, 128281. https://doi.org/10.1016/J.BIORTECH.2022.128281.
Zhao, J., Li, C., Fan, X., Liu, H., Liu, Z., Zhang, J., Sun, Z., Chu, W., 2023. Design and synthesis of Brønsted-Lewis acidic tetraimidazolyl ionic liquids for efficient catalytic conversion of glucose to 5-hydroxymethylfurfural in water/1-octanol. Appl. Catal. Gen. 649. https://doi.org/10.1016/j.apcata.2022.118981.
Zhou, H., Zhu, J.Y., Luo, X., Leu, S.Y., Wu, X., Gleisner, R., Dien, B.S., Hector, R.E., Yang, D., Qiu, X., Horn, E., Negron, J., 2013. Bioconversion of beetle-killed lodgepole pine using SPORL: Process scale-up design, lignin coproduct, and high solids fermentation without detoxification. Ind. Eng. Chem. Res. 52, 16057–16065. https://doi.org/10.1021/ie402873y.
Zhu, W., Houtman, C.J., Zhu, J.Y., Gleisner, R., Chen, K.F., 2012. Quantitative predictions of bioconversion of aspen by dilute acid and SPORL pretreatments using a unified combined hydrolysis factor (CHF). Process Biochem. 47, 785–791. https://doi.org/10.1016/j.procbio.2012.02.012.
Zhu, L., Tang, W., Ma, C., He, Y.-C., 2023. Efficient co-production of reducing sugars and xylooligosaccharides via clean hydrothermal pretreatment of rape straw. Bioresour. Technol. 388, 129727. https://doi.org/10.1016/j.biortech.2023.129727.
Zikria, R., 2022. Outlook Komoditas Perkebunan Kelapa Tahun 2022.